JOURNAL OF GEOPHYSICAL RESEARCH, VOL. 103, NO. B10, PAGES 23,795–23,812, OCTOBER 10, 1998

Crustal structure of the northwestern Vizcaino block and Gorda Escarpment, offshore northern California, and implications for postsubduction deformation of a paleoaccretionary margin

Beate Leitner[1] and Anne M. Tréhu

College of Oceanic and Atmospheric Sciences, Oregon State University, Corvallis

Nicola J. Godfrey[2]

Department of Geophysics, Stanford University, Stanford, California

Abstract. The Vizcaino block is an anomalously shallow region of the western U.S. continental margin located southwest of the Mendocino triple junction. It originated as part of the accretionary prism of the North America plate and was transferred to the Pacific plate in the Miocene as the Pacific-North America plate boundary migrated ~130 km eastward, forming the Gorda Escarpment at its northern boundary. We present hybrid crustal models for the northwestern part of the Vizcaino block derived from marine seismic and gravity data. The velocity and density structure of the northwestern Vizcaino block are compatible with paleoaccretionary complex material similar to San Simeon/Patton terrane overlying oceanic crust or a mafic layer. The most significant result of our modeling is an abrupt increase in Moho dip from ~5° to ~20-30° beneath the western edge of the Oconostota ridge along the northwestern margin of the Vizcaino block. This Moho dip is steeper than observed anywhere along the Cascadia subduction zone, indicating postsubduction deformation. We suggest that the paleotrench was deformed by compression, which reactivated preexisting thrust faults in the upper crust and thickened the crust within this apparent weak zone. At least part of the deformation predates late Pliocene Pacific-North America plate convergence and may result mainly from north-south compression between the Pacific-Juan de Fuca plates across the Mendocino transform fault. North-south compression continues today and may dynamically support the uplifted northern margin of the Vizcaino block, although the primary locus of deformation shifted to the relatively weak Gorda plate sometime prior to 3 Ma.

1. Introduction

The active Cascadia margin north of the Mendocino triple junction has a shallow-dipping Moho and base to the accretionary prism. In contrast, results from several transects across the paleoaccretionary prism making up the California margin show steeply dipping lower crust and Moho segments [e.g., *Tréhu*, 1991; *Meltzer and Levander*, 1991; *Howie et al.*, 1993; *Holbrook et al.*, 1996; *Miller et al.*, 1992, 1996], indicating postsubduction deformation. Marine seismic and gravity data from the Mendocino Triple Junction Seismic Experiment [*Tréhu et al.*, 1995] allow further investigation of the tectonic process causing this deformation in the northwestern Vizcaino block. The hybrid velocity and density crustal models derived in this study image the lower crustal deformation along strike and address the question of why deformation is focused along the seaward part of the accretionary wedge. Resolution of the Moho dip and its trend is better in this study than in many of the earlier studies because of the range of strikes along which this feature has been sampled.

1.2. Vizcaino Block

The Vizcaino block forms an unusually wide, triangular-shaped, shallow region on the continental margin (Plate 1a) offshore northern California whose tectonic history and basement structure has been the subject of considerable speculation. It is bounded by the Mendocino transform fault to the north, the San Andreas fault zone to the east, and the Navarro discontinuity to the southwest, and it approximately follows the continental slope and change of trend in magnetic anomalies at its western margin (for a summary, see *McCulloch* [1987a, b, 1989]). Its western margin is characterized by a buried basement high, known as the Oconostota ridge, which is approximately parallel to topographic contours.

Vizcaino block basement is juxtaposed against the onshore King Range terrane (middle Miocene [*McLaughlin et al.*, 1982]) and coastal Franciscan belt (Cretaceous to Eocene accretionary complex [*Blake and Jones*, 1981]) along the San Andreas fault, and abuts against the Salinian terrane (Cretaceous plutonic terrane [*Mattinson*, 1978]) and Franciscan or San Simeon

[1]Now at Institute of Geological and Nuclear Sciences, Dunedin, New Zealand.

[2]Now at Department of Earth Sciences, University of Southern California, Los Angeles.

Paper number 98JB02050.
0148-0227/98/98JB-02050$09.00

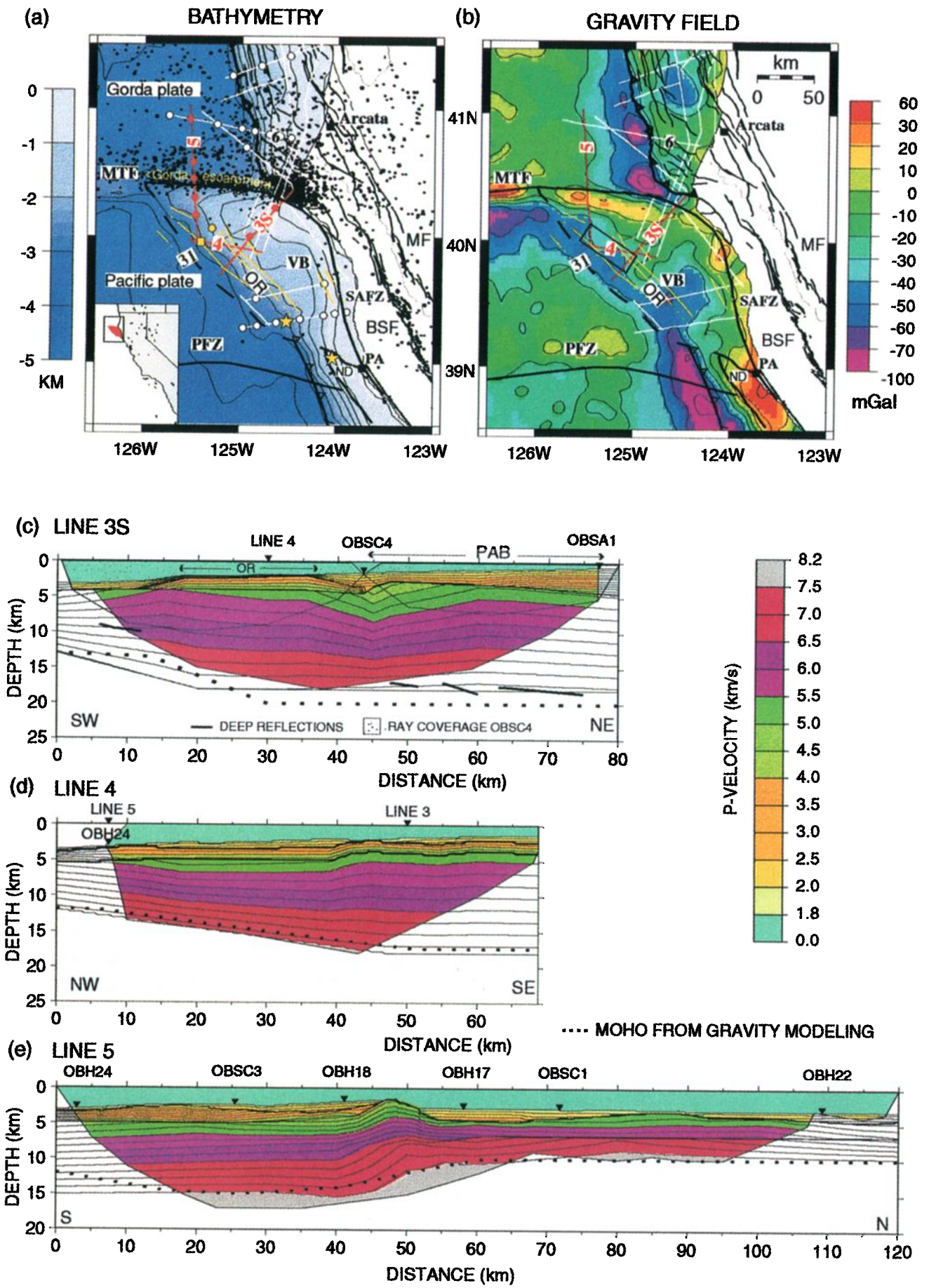
(a)
BATHYMETRY
Gorda plate
Pacific plate
MTF
Gorda escarpment
Arcata
MF
VB
OR
SAFZ
BSF
PFZ
PA
AND
KM
0
-1
-2
-3
-4
-5
41N
40N
39N
126W
125W
124W
123W
(b)
GRAVITY FIELD
km
0 50
ND
mGal
60
30
20
10
0
-10
-20
-30
-40
-50
-60
-70
-100
(c) LINE 3S
LINE 4
OBSC4
PAB
OBSA1
OR
SW
NE
DEEP REFLECTIONS
RAY COVERAGE OBSC4
DEPTH (km)
DISTANCE (km)
(d) LINE 4
LINE 5
LINE 3
OBH24
NW
SE
(e) LINE 5
OBH24
OBSC3
OBH18
OBH17
OBSC1
OBH22
S
N
P-VELOCITY (km/s)
8.2
7.5
7.0
6.5
6.0
5.5
5.0
4.5
4.0
3.5
3.0
2.5
2.0
1.8
0.0
MOHO FROM GRAVITY MODELING

terranes (Cretaceous-Oligocene accretionary complex [*McLaughlin et al.*, 1994]) at the Navarro discontinuity. The Vizcaino block is presently part of the Pacific plate and is migrating northward relative to the North America plate along the present-day San Andreas transform fault system [*Atwater*, 1970, 1989]. At present, much of the transform motion in the San Andreas fault system appears to be taken up in the Coast Range east of the San Andreas fault along the Maacama and Bartlett Springs faults [*Castillo and Ellsworth*, 1993]. Seismicity in the offshore region, an indication of present-day tectonic deformation, is concentrated along the Mendocino transform fault and within a triangular region in the southeast corner of the Gorda plate adjacent to the Vizcaino block (Plate 1a). The Vizcaino block therefore appears to represent a rigid part of the Pacific plate.

The Vizcaino block basement is believed to have formed in an accretionary prism. This conclusion is supported by lithologic basement samples from four localities in the western part of the Vizcaino block [*McCulloch*, 1987a; *McLaughlin et al.*, 1994], a deep reflection interpreted to be the top of the subducted plate beneath the western margin [*McCulloch*, 1987a; *Henstock et al.*, 1996, 1997; *Godfrey*, 1997], and multiple basement ridges throughout the western part of the Vizcaino block (Plate 1a; yellow lines) that have been interpreted as blind thrusts similar to those observed in accretionary complexes [*Godfrey*, 1997]. The satellite-derived free-air gravity anomaly data over the western margin show a gravity low (Plate 1b), typical for a subduction zone trench. This low, however, is less prominent than the observed gravity low along the Cascadia trench north of the Mendocino transform fault or the paleotrench south of the Vizcaino block in central California (Plate 1b). One objective of this project was to determine whether this is entirely due to differences in the accretionary prism geometry or if structural deviations from a typical paleotrench boundary are required in the underlying crust.

1.2. Gorda Escarpment

The morphology of the Mendocino transform fault changes at about 126°W. East of 126°W, the Mendocino transform fault is at the base of the Gorda Escarpment, a steep, north facing escarpment where the Vizcaino block is elevated up to 1.5 km above the Gorda plate seafloor (Plate 1a). This topographic step is opposite of what is predicted from the age difference between the Pacific (old) and Gorda (young) plates. West of 126°W, the seafloor of the Pacific plate is, on average, 1 km deeper than the adjacent Gorda seafloor, consistent with the age and density contrast between the two plates [*Engebretson et al.*, 1985], and the transform is immediately north of a 5-15 km-wide ridge known as the Mendocino Ridge. Basalt cobbles dredged from the ridge and submersible observations indicate that the Mendocino Ridge was once above sea level [*Krause et al.*, 1964; *Duncan et al.*, 1994] and has since subsided. Ages of rock samples from the Mendocino Ridge west of 126°W range between 7 and 22 Ma, indicating that Gorda plate material was obducted onto the Pacific plate [*Duncan et al.*, 1994]. In contrast, the only dated sample from the Gorda Escarpment is Cretaceous [*Fisk et al.*, 1993]. These observations suggest that the evolution of the Gorda Escarpment is connected with the development of the Vizcaino block and may have an uplift and subsidence history that is different from that of the Mendocino Ridge west of 126°W. A second objective of this study was to determine whether the basement ridge along the Gorda Escarpment is gravitationally compensated by a crustal root.

1.3. Plate Tectonic History

The present-day structure of the Vizcaino block and Gorda Escarpment is the integrated result of plate boundary processes since the Oligocene. Numerous workers have reconstructed the plate boundary evolution in time and space based on offshore magnetic anomalies, fault offsets in California, and other geologic constraints [e.g., *Atwater*, 1970; *Graham and Dickinson*, 1978; *Engebretson et al.*, 1985; *Atwater and Severinghaus*, 1989; *Drake et al.*, 1989; *Sedlock and Hamilton*, 1991; *Fernandez and Hey*, 1991; *Lonsdale*, 1991; *Wilson*, 1993; *McLaughlin et al.*, 1994; *Nicholson et al.*, 1994; *Bohannon and Parsons*, 1995; *McCrory et al.*, 1995]. The four important stages of plate boundary evolution in the history of the Vizcaino block are subduction, extension, transfer to the Pacific plate, and Pacific plate motion (Figure 1). The Farallon plate subducted beneath the North American continent until about 27-25 Ma (Figure 1a) , when the Pacific-Farallon ridge reached the trench. Spreading and subduction of the ridge beneath the accretionary

Plate 1. (top) Map of the Mendocino triple junction region. Red (data presented in this paper) and white lines mark the R/V *Ewing* ship tracks along which seismic and gravity data were collected during the 1994 Mendocino triple junction seismic experiment. Gray line is a seismic reflection line of 1977 vintage shown in Figure 9. SAFZ, San Andreas fault zone; MTF, Mendocino transform fault; ND, Navarro discontinuity; PFZ, Pioneer fracture zone; VB, Vizcaino block, OR, Oconostota ridge, PA, Point Arena; BSF, Bartlett Spring fault; MF, Maacama fault. Faults to the east of the SAFZ and the Cascadia trench are from *Castillo and Ellsworth* [1993]. The western margin of the Vizcaino block is shown as a dashed line [after *McCulloch*, 1987a]. Open triangles mark the approximate location of the paleotrench south of the ND; solid triangles mark the position of the Cascadia trench. (a) Bathymetry (National Geophysical Data Center CD-Rom release 1.0, Geophysics of North America). Basement sample locations shown as yellow stars [*McCulloch*, 1987a] and basement ridges after *Godfrey* [1997] shown as yellow lines. DSDP Site 173 is marked by a yellow square, ODP Site 1022 is marked by a yellow circle. Solid dots are earthquakes with $M>3$ (northern California earthquake data center, 1970-1996). The inset locates the map region and Vizcaino block in California. (b) Global marine gravity data [*Sandwell and Smith*, 1997]. The solid box marks the region of the Moho kink discussed in this study. (bottom) Velocity models of lines 3S, 4 and 5 incorporating basement depth and sediment velocities from MCS data. The portion of the model constrained by seismic data is colored. OR, Oconostota ridge; PAB, Point Arena basin. (c) Velocity model of line 3S. Note the absence of a continuous deep reflector between km 15 and 45. In this region basement topography is rough and energy gets scattered in the deeper section. (d) Velocity model of Line 4. Only one instrument recorded the data, and the model is constrained by the intersecting lines 3 and 5 velocity models. (e) Velocity model of line 5. The crust south of the Gorda Escarpment is twice as thick as to the north and increases abruptly beneath the Gorda Escarpment.

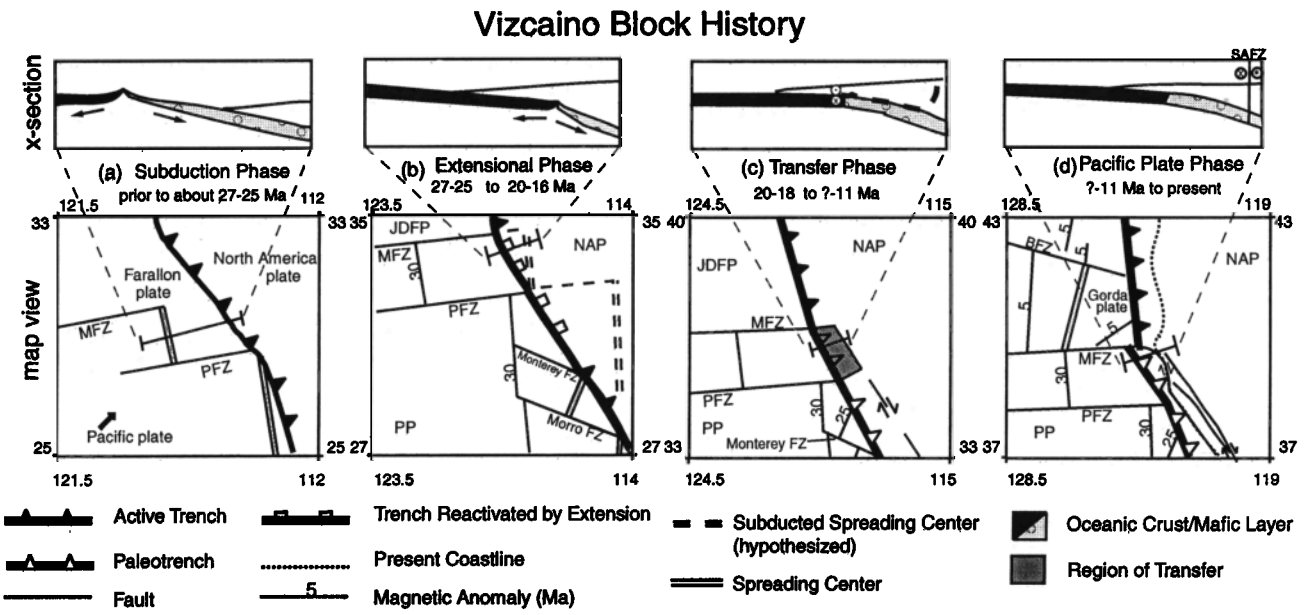

Figure 1. Cartoon of the plate boundary evolution (adapted from *Bohannon and Parsons* [1995] at 30, 20, 10, and 0 Ma) highlighting the important phases in Vizcaino block history since the Oligocene. Locations of the cross sections are indicated by the solid line on the map view. Ages in Ma are upper and lower bounds for the given processes. MFZ, Mendocino fracture zone; PFZ, Pioneer fracture zone; JDFP, Juan de Fuca plate; NAP, North America plate; PP, Pacific plate. (a) Subduction phase; subduction of the Farallon plate beneath the North-American continent until the ridge collided with the trench about 27-25 Ma. The Vizcaino block is part of the accretionary wedge at the western margin of the North America plate north of the Mendocino fracture zone. (b) Extensional phase; following ridge collision about 27-25 Ma, the Pacific plate and the Pacific-Farallon ridge likely continued subduction and ridge spreading [*McLaughlin et al.*, 1996] until about 20-16 Ma. The ridge possibly continued to move eastward and could have caused relative high heat flow, magmatic underplating and the formation of the Point Arena basin in its wake. (c) Transfer phase; offshore transform initiated 20-18 Ma possibly on a detachment surface beneath the accretionary wedge (dashed line in cross section) and connected the Mendocino fracture zone with the northward extension of the Pacific-Farallon ridge system to the south by initiating the San Andreas-Pilarcitos fault system [after *McLaughlin et al.*, 1996]. The detachment region beneath the accretionary wedge marked in gray grows eastward with time. At about 12-10 Ma, the San Andreas fault is the master fault and the Vizcaino block is now part of the Pacific plate. (d) Pacific plate phase; the Vizcaino block moves with the Pacific plate along the San Andreas fault system. About 3.5 Ma, near Point Arena, the San Andreas fault changed its trend to a more northerly direction responding to a clockwise change of Pacific-North America relative plate motion.

prism may have continued until 20-16 Ma [*Severinghaus and Atwater*, 1990; *Bohannon and Parsons*, 1995; *McLaughlin et al.*, 1996] (Figure 1b).

Between 20 and 12 Ma, there was a change from oblique subduction to transform motion on the San Andreas fault system. The evolution of transform motion in time and space during this period is poorly constrained. *McCrory et al.* [1995] speculated that between 20 and 16 Ma, transform motion initiated along a subsurface detachment at the slab-accretionary complex interface and that this low-angle transform boundary propagated eastward and upward (Figure 1c) forming the Gorda Escarpment in its wake. It remains uncertain if the eastward migration of the plate boundary was a continuous process through time or occurred in distinct steps [e.g., *Dickinson and Snyder*, 1979; *McCulloch*, 1987b; *Drake et al.*, 1989; *Griscom and Jachens*, 1989; *Sedlock and Hamilton*, 1991; *Smith et al.*, 1993; *McLaughlin et al.*, 1994, 1996].

About 12-10 Ma the primary locus of transform motion apparently shifted to the Pilarcitos/San Andreas fault system [*McLaughlin et al.*, 1996]. *Griscom and Jachens* [1989] propose that an offshore transform fault west of the present-day San Andreas fault zone was active until about 5 Ma. The apparent absence of strike-slip type deformation in seismic reflection data from the 6-10 Ma Delgada fan [*Drake et al.*, 1989] and underlying late Miocene sediments that overlie the Vizcaino block [*Hoskins and Griffiths*, 1971; *McCulloch*, 1987a; *Drake et al.*, 1989; *Godfrey*, 1997; *Ondrus*, 1997], however, has been used to argue against this interpretation. *Godfrey et al.* [this issue] present evidence that the present-day Mendocino triple junction may have been at its present location relative to the Mendocino transform fault significantly earlier than 11 Ma.

The uplift of both the Mendocino Ridge and Gorda Escarpment may have been a result of compressional stresses across the transform caused by changes in relative plate motion, [e.g., *Riddihough*, 1984; *Wilson et al.*, 1984; *Duncan and Clague*, 1985; *Cox and Engebretson*, 1985; *Wilson*, 1988, 1993] and by differences in thermal and viscoelastic properties of the adjacent oceanic lithospheres [*Bonatti*, 1978]. The latter are partly controlled by the age difference between the plates, which changed polarity at about 12 Ma [*Engebretson et al.*, 1985]. North-south compression increased considerably after the inception of the Blanco transform (about 6 Ma) and continues to

the present-day [*Wilson*, 1993]. Part or all of the present-day north-south compression is absorbed by the Gorda plate, where the curvature of magnetic patterns and shorter magnetic anomalies on the east side versus the west side of the Gorda ridge indicate internal deformation [e.g. *Silver*, 1971; *Riddihough*, 1980; *Wilson*, 1986, 1989; *Stoddard*, 1987; *Denlinger*, 1992]. That the morphology of the Gorda Escarpment is different from that of the Mendocino Ridge west of 126°, whereas the same tectonic forces are active, suggests that it is strongly affected by the crustal structure of the Vizcaino block.

2. Data Acquisition, Processing, and Modeling

We present large-aperture seismic and gravity data collected over the northwestern part of the Vizcaino block, the Gorda Escarpment, and the Gorda plate during the 1994 phase of the Mendocino Triple Junction Seismic Experiment [*Tréhu et al.*, 1995]. The R/V *Ewing* recorded multichannel seismic (MCS), potential field and bathymetric data along 14 profiles. Results from three of these profiles are presented in this study (Plate 1a). Four ocean bottom seismographs (OBS) and four ocean bottom hydrophones (OBH), deployed from the R/V *Wecoma*, recorded shots from the R/V *Ewing* tuned air gun array along lines 3S, 4, and 5 (Plate 1a, marked in red). We construct hybrid crustal models using the MCS data to constrain sediment thickness along the profiles, the large-aperture data to constrain the P wave velocity and thickness of the crust where permitted by the ray coverage, and gravity data to extend constraints on the geometry of the lower crust and Moho. Details of MCS processing and interpretation are discussed elsewhere [*Godfrey*, 1997; *Godfrey et al.*, this issue; T. Henstock, personal communication, 1997; A. S. Meltzer, personal communication, 1997]. Magnetic field data are not discussed in this paper since the magnetic field variation over the Vizcaino block is small along lines 3S, 4, and 5 south of the Mendocino transform fault. The magnetic field of the Gorda Escarpment where crossed by line 5 is well modeled assuming an average susceptibility of oceanic crust. Directly north of the Mendocino Ridge, magnetic lineations from the Gorda crust trend obliquely to line 5, and two-dimensional (2-D) modeling is not valid.

2.1. Modeling the Large-Aperture Seismic Data

Large-aperture data coverage is best on line 5, along which 6 instruments recorded data (Plate 1a). At the intersection of lines 4 and 5, OBH 24 recorded air gun shots from both lines. On line 3S only 2 of 3 instruments deployed recorded data. Air gun shots on lines 3S, 4, and the middle section of line 5 were shot at 20 s intervals (about 50 m) to optimize the MCS data. This resulted in bands of previous shot noise (PSN) that interfere with crustal arrivals in the OBH/OBS record sections (Figure 2). Shot spacing at both ends of line 5 was 50 s (about 130 m), which is preferable for large-aperture data when seafloor depths are greater than 1000 m [*Christeson et al.*, 1996]. Although the signal-to-noise ratio on the OBHs was generally higher than on the OBSs, the OBHs were more strongly affected by PSN (Figure 2). PSN could be reduced, but not eliminated, by applying an F-k filter to the data after shifting the data to align traces along the previous shot instant [*Christeson et al.*, 1996].

After applying a time domain band-pass filter (4-30 Hz), gain amplification as a function of range and a 6.5 kms^{-1} reduction velocity to the OBHs/OBSs data, and after adding 2 adjacent traces when data were shot at a 20 s interval, travel-time picks were digitized from the record sections. A strong multiple (marked m, Figure 2) arriving with a time delay equal to the two-way travel time (twtt) through the water column above the instrument is apparent on all instruments. The amplitude of this arrival is often stronger than the first arrival, and it was used to verify and extend the range of first-arrival picks.

A starting model for 2-D inversion of travel times [*Zelt and Smith*, 1992] for line 3S utilized basement depths taken directly from a depth-migrated reflection profile [*Henstock et al.*, 1996]. The starting models for lines 4 and 5 were constructed from bathymetric and time-migrated MCS data. For lines 4 and 5, seafloor to basement travel times were converted to depth assuming a constant velocity gradient of 0.7 $kms^{-1}km^{-1}$ and a constant velocity of 1.8 kms^{-1} at the top of the sediment layer. This velocity gradient is an average of the velocity gradients obtained from 1-D travel time modeling of near-offset data for the line 5 instruments. In addition, the velocity model at the northern end of line 5 was constrained in the inversion by velocity information from line 6 [*Tréhu et al.*, 1995].

Velocity models (Plate 1c-1e) were determined through an iterative forward/inverse modeling approach in which the initial inversion was performed for a three layer model (water, sediment, and crust) with velocities in the water and sediment layers fixed and velocity nodes to be determined by inversion placed at 20-km intervals along the top and bottom of the crustal layer. Because velocities between nodes increase linearly, velocity discontinuities and gradient changes in the crust were modeled by introducing additional layers, and the data were reinverted after the addition of each layer.

The introduction of an upper crustal layer, allowing relatively low velocities and a high-velocity gradient in the upper basement of the Vizcaino block, reduced the travel time misfit for lines 3 and 5. Constraints on the velocity and thickness of the lower crust of the Gorda plate on line 5 were included as indicated by results from line 6, where reversed arrivals are observed from the lower crust and upper mantle [*Tréhu et al.*, 1995]. The modeled *Pn* and *PmP* arrivals were not included in the inversion. The Moho depth of lines 3 and 4 were constrained by MCS and gravity data, where possible. The final models for lines 3S, 4, and 5 contain two, one, and three crustal layers, respectively. Final travel time misfits are summarized in Table 1.

2.1.1. Line 3S. Line 3S lies entirely within the Vizcaino block, extending diagonally from its western boundary at 125.2°W, 39.7°N to the coast near Cape Mendocino (Plate 1a). The profile is orthogonal to the Oconostota ridge and mapped basement ridges, providing a cross section of the Vizcaino block. Water depth decreases gradually from west (3 km) to east (0.5 km) along the profile, with a relatively rapid decrease between km 13 and 18 (the seaward edge of the Vizcaino block) (Figure 3a). The basement is shallowest between km 18 and 38, corresponding to the Oconostota ridge. A deep sedimentary basin (the Point Arena basin) overlies the eastern end of the profile, and sediments thicken west of the Oconostota ridge.

For this profile, we focus on using limited seismic data in conjunction with gravity data to explore a range of possible models for the Moho configuration beneath the Oconostota ridge. This work complements efforts by *Henstock et al.* [1996] to determine structure beneath the triple junction region using MCS, OBS, and onshore-offshore data along two long profiles that cross approximately at the triple junction. We present a detailed analysis of a subset of the seismic data used for their model.

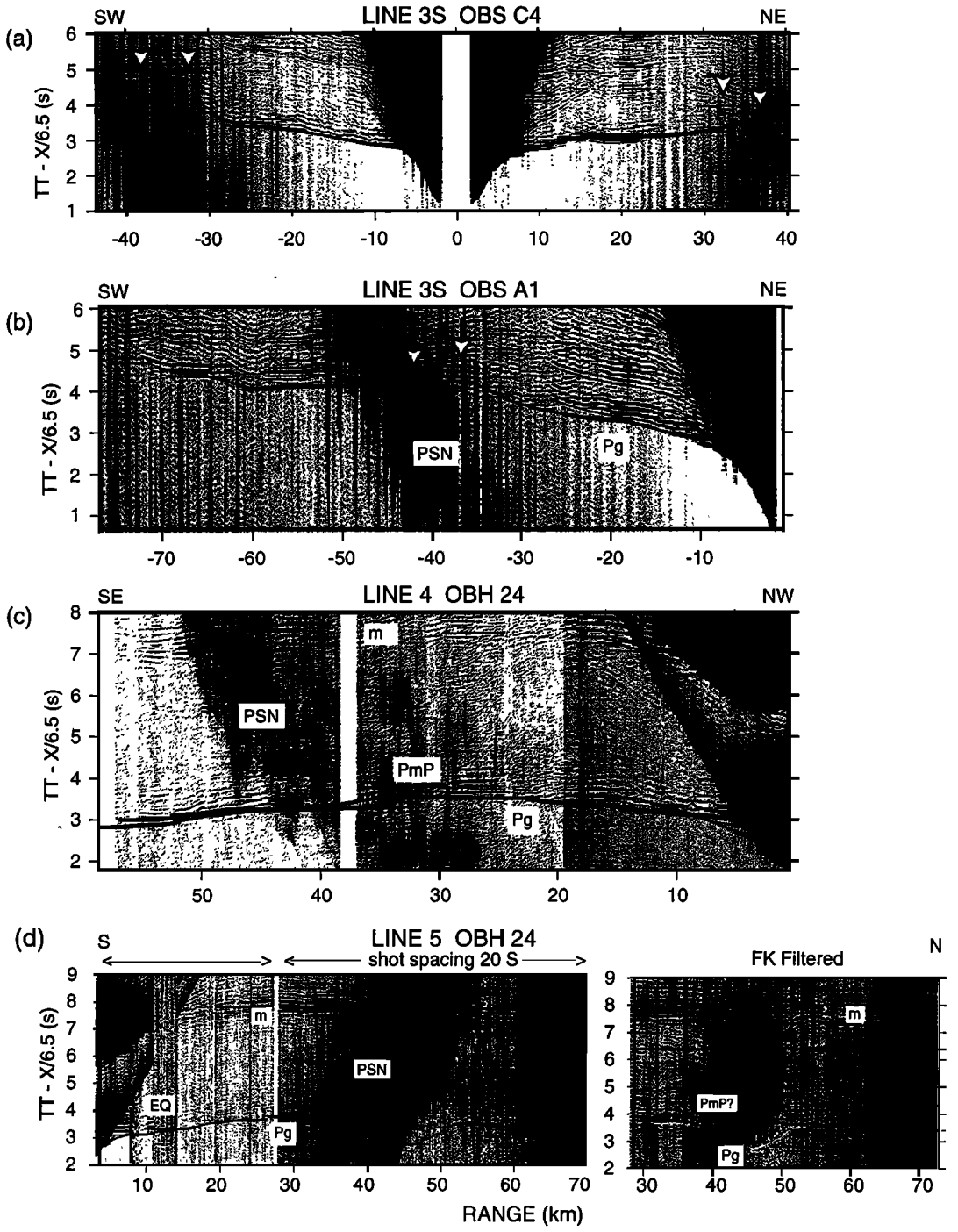

Figure 2. Processed record sections (see text for details) of ocean bottom instruments recording (a) and (b) line 3S, (c) line 4 and (d)-(i) line 5 MCS air gun shots. Shot spacing for line 5 instruments is indicated at top. PSN, previous shot noise; m, water multiple; EQ, M_w 5.0 earthquake located offshore Petrolia, California [*Braunmiller et al.*, 1997]. Calculated arrival times for the velocity models in Plate 1 (c)-(e) are shown by the solid lines. White arrows indicate possible lower crustal or Moho reflections not constrained by our line 3S velocity model. Possible mantle arrivals on OBS C3 and OBH 18 (marked '?') beneath the Gorda plate are obscured by PSN.

The large-aperture seismic data only sparsely sample the crust (Plate 1c). OBS C4 (Figure 2a) recorded diving waves (*Pg*), sampling the upper 4-6 km of basement. A possible wide-angle reflection from the mid crust beneath the northeastern end of the line is marked by white arrows (Figure 2a) and is consistent with onshore-offshore observations, which require a thick layer of high-velocity lower crust at a depth of 9 km beneath the northeastern end of line 3S [*Henstock et al.*, 1996]. OBS A1 (Figure 2b) recorded *Pg* arrivals to an offset of 75 km, sampling the lower crust to a depth of 18 km. Ray coverage in the lower crust is limited to km 30 to 60 in the model. An arrival that may represent a reflection from either the top of the oceanic crust or

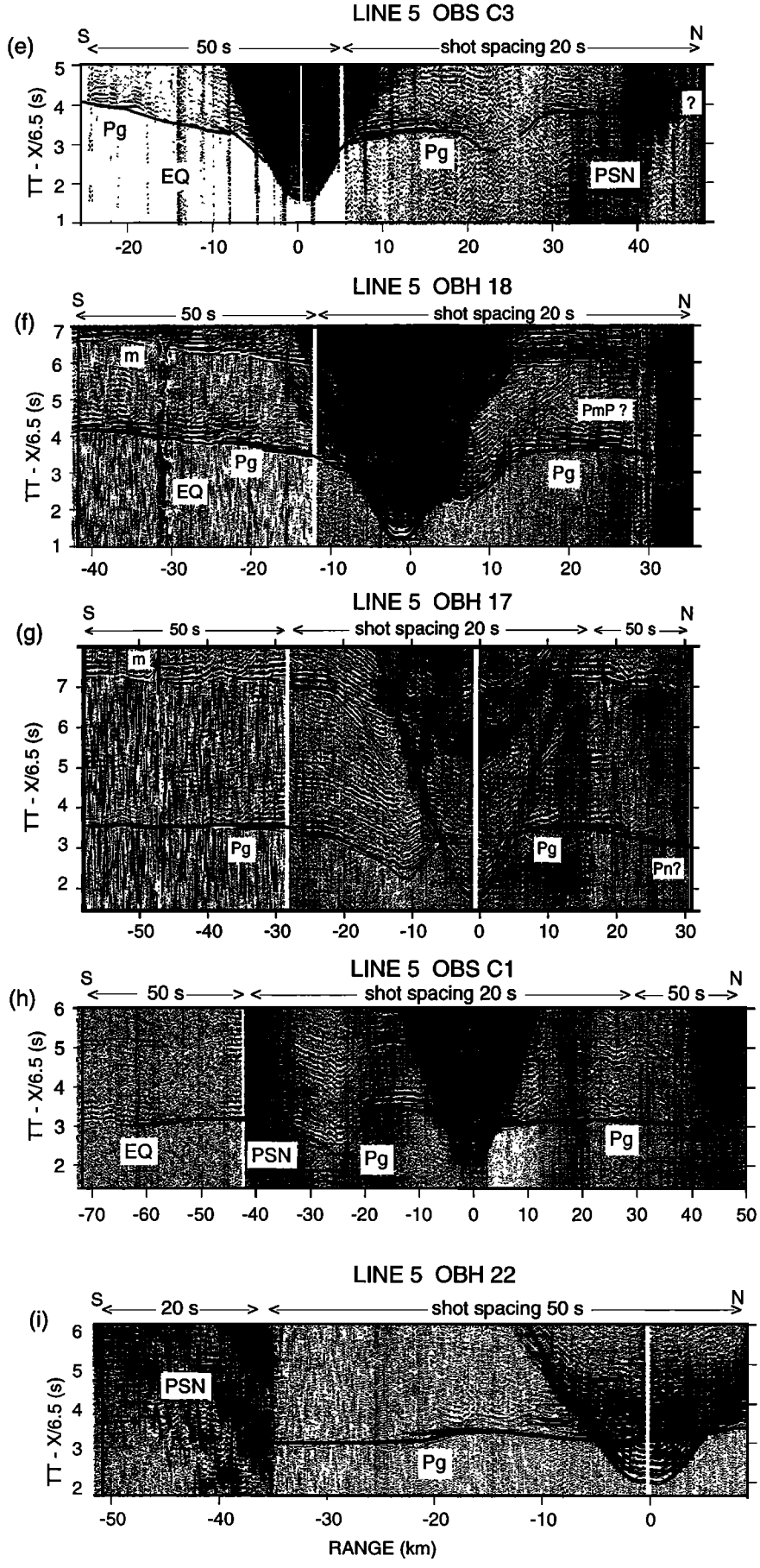

Figure 2. (continued)

Table 1. RMS Values of Velocity Models based on *Pg* Arrivals (Plate 1c-1e) and Gravity Models (Figure 7)

Models	Line 3S	Line 4	Line5
Velocity model	0.13	0.077	0.097
Gravity models			
Model I	2.83	3.5	3.1
Model II	1.78		2.87
Model III	1.94		

Misfits in s (velocity) and mGal (gravity).

from the Moho is marked by white arrows (Figure 2b), but due to our limited ray coverage in the lower crust, we cannot uniquely model it.

A lateral velocity change in the basement rocks at about km 40 to 50 is required to model the near-range arrivals of OBS C4, which are only slightly asymmetric despite a pronounced decrease in sediment thickness west of the instrument (Figure 3a). In order to match these arrivals, a 2-km-thick layer with velocities of 3.5-4.5 kms^{-1} was added just beneath the basement west of OBS C4 (Plate 1c). The thickness of and velocity in this layer agree with an intermediate velocity layer modeled at the southern end of line 5 and on the western part of line 4 (see discussion of these lines below). Beneath this depth, velocities increase approximately linearly with depth. A dip in the velocity contours beneath OBS C4 may be an artefact of uncertainties in the detailed configuration of the base of the overlying layer.

2.1.2. Line 4. Line 4 extends for 70 km across the northwestern part of the Vizcaino block, crossing line 5 at km 7 and line 3 at km 50. Almost the entire line lies within the region of the Oconostota ridge. MCS data define the top of the basement (Figures 3b and 3c), and no deeper reflections are observed. Basement topography is rough, and the general appearance of the data is similar to that of line 3S west of km 40 and line 5 south of the Gorda Escarpment.

OBH 24, located at the intersection of line 4 with line 5, recorded *Pg* and possible *PmP* and *Pn* arrivals to an offset of 60 km (Figure 2c). With only one receiver, we cannot resolve dipping structure and velocity gradients uniquely, although comparison with models for lines 3S and 5 help constrain the model. The resulting velocity model (Plate 1d) fits the data well (Table 1). Beneath the sediments, an intermediate velocity layer (3.5-4.5 kms^{-1}) of 2 km thickness overlies a layer with velocities of 5.0 to 7.4 kms^{-1}.

2.1.3. Line 5. Four OBHs and two OBSs recorded air gun shots along the 120-km-long line 5 (Plate 1a). South of the Gorda Escarpment, the profile lies in the Vizcaino block and the seafloor rises from 3 km at the southern end of the profile to 1.5 km depth at the Mendocino Ridge. It then drops steeply to the 3-km-deep Gorda plate ocean floor. MCS data constrain the sediment thickness along the profile (Figure 3d). Sediment thickness increases toward the ridge from the south between km 20 to 40 and pinches out against the ridge crest. North of the ridge, the basement is offset by large faults that cut through the sediment and, in at least one case, offset the seafloor. No deep reflections are observed.

Rapid bathymetric and sediment thickness changes dominate the record sections (Figures 2d-2i). Modeled arrivals in the Vizcaino block are diving waves (*Pg*) through the crust (OBH 24, OBS C3, OBH 18, OBH 17 south, and OBS C1 south). Shots from the southern end were recorded as far north as OBS C1 (offset of 76 km). F-k filtering enabled us to verify travel time picks between offsets of 28-45 km on OBH 24, where previous shot noise (PSN) obscured the arrivals on the unfiltered data (Figure 2d). The final velocity model south of the ridge (Plate 1e) has a 1.5-km-thick intermediate velocity layer (2.5-4.5 kms^{-1}) that is underlain by rocks in which velocity increases approximately linearly from 5 to 7.4 kms^{-1}. The thick crust extends beneath the Mendocino Ridge to the Gorda Escarpment, north of which crustal thickness decreases abruptly.

The northern instruments were in an area of rough basement topography, leading to large diffractions, considerable scattering of seismic energy, and maximum observed offsets of about 30 km (OBH 22, OBS C1 north, OBH 17 north). Instruments north of the ridge are modeled by upper crustal velocities of 5-6 kms^{-1} overlying a lower crust with velocities of 6.5-7.6 kms^{-1}. The mid-crustal boundary is at 6.7 km depth, and the Moho is at 10 km depth (Plate 1e). Moho depth is constrained primarily by results from line 6 [*Tréhu et al.*, 1995] and is consistent with a possible *PmP* arrival on OBH 18 and *Pn* arrival on OBH 17 (Figures 2f and 2g).

We can compare our velocity model at the southern end of line 5 to results from the Deep Sea Drilling Project (DSDP) Site 173 at the intersection of lines 4 and 5 (Figure 4). The 0.4-km-thick sediment layer in our velocity model is in agreement with the drilling results [*Kulm et al.*, 1973]. The top of our intermediate velocity layer has velocities of 2.5-4.5 kms^{-1} and coincides with the recovery of andesitic basalt at the bottom of the drill hole at 330 m. The velocities in this 1.5-km-thick layer are compatible with velocities of highly porous basalt or consolidated sediments and are observed in Franciscan/San Simeon terrane offshore central California [*Howie et al.*, 1993; *Holbrook et al.*, 1996]. The lateral extend of the andesitic basalt found in DSDP Site 173 remains uncertain.

We used elastic finite difference wave field modeling (code developed by *Rodrigues and Mora* [1992], adapted by *Lendl* [1996], summary by *Lendl et al.* [1997]), to verify the model along line 5. For this calculation, the velocity model was gridded at a 50-m spacing, and an explosive point source with a

Figure 3. (a) Line 3S bathymetry from ship data and top of basement from depth migrated MCS data. (b) Migrated multichannel seismic data along MCS line 4 show several basement ridges. Sediment horizons above the ridges are deformed and interrupted. (c) Line 4 bathymetry from ship measurements and top of basement from MCS data along line 4 constrain the velocity and gravity models. (d) Migrated near-trace data for line 5 shown with amplitudes corrected for spherical spreading. The top of the basement is well defined along the entire profile. The pattern of uplift and tilting of sediments on the Mendocino Ridge is similar to that reported by *Silver* [1971]. A more detailed discussion of stratigraphy based on MCS data is presented by *Godfrey et al.* [this issue]. (e) Line 5 bathymetry from ship data and top of basement from time migrated MCS data (A. S. Meltzer, unpublished data, 1997). See text for details of the twtt to depth conversion. Bathymetry and sediment thickness changes between 0 and 2 km along the profile.

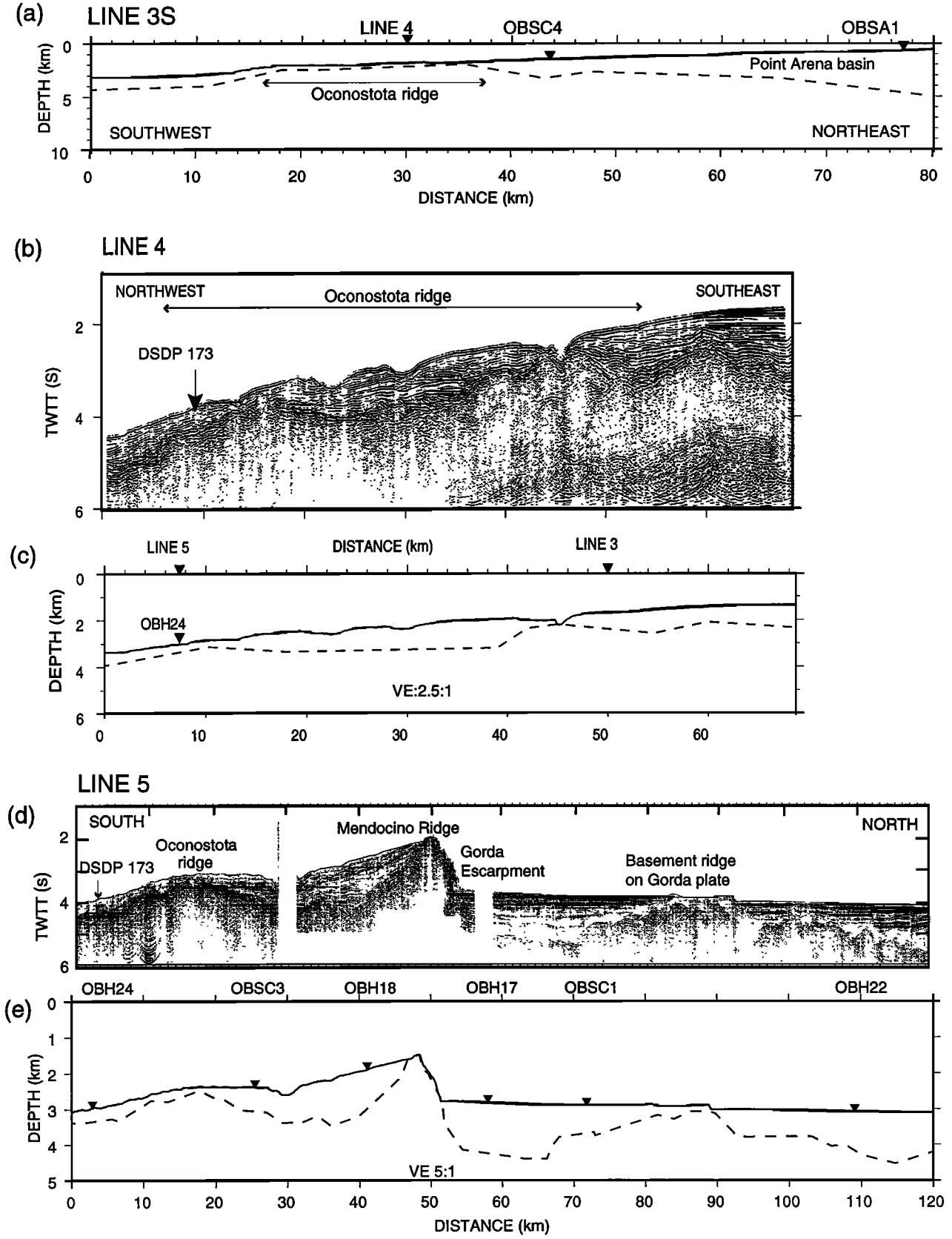
(a)
LINE 3S
LINE 4
OBSC4
OBSA1
Point Arena basin
Oconostota ridge
SOUTHWEST
NORTHEAST
DEPTH (km)
DISTANCE (km)
(b)
LINE 4
NORTHWEST
Oconostota ridge
SOUTHEAST
DSDP 173
TWTT (S)
(c)
LINE 5
DISTANCE (km)
LINE 3
OBH24
VE:2.5:1
DEPTH (km)
LINE 5
(d)
SOUTH
NORTH
Oconostota ridge
DSDP 173
Mendocino Ridge
Gorda Escarpment
Basement ridge on Gorda plate
TWTT (s)
OBH24
OBSC3
OBH18
OBH17
OBSC1
OBH22
(e)
VE 5:1
DEPTH (km)
DISTANCE (km)

Figure 3.

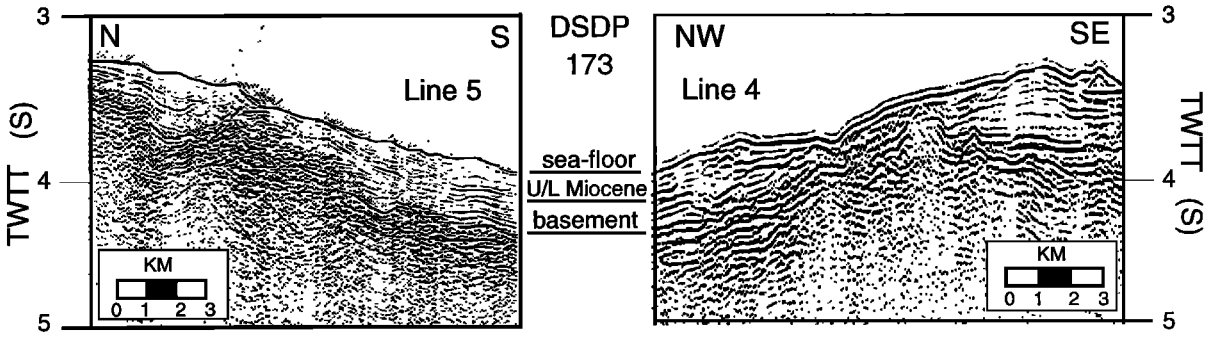

Figure 4. Blow up of MCS data for lines 4 and 5 at their intersection and DSDP Site 173. Depth of the middle/late Miocene boundary converted from twtt is approximate, and no distinct sediment horizon is apparent.

maximum frequency of 10 Hz was put at each instrument location. The wave field was recorded at 50-m intervals on the surface (i.e., the opposite of the actual experiment geometry). The synthetic record section for instrument OBH 17 shows a close match to the data (Figures 5 and 2g). The travel time advance resulting from propagation through the ridge matches the data satisfactorily, and the relative amplitudes of direct waves, multiples, shear and converted waves are reproduced. We conclude that our model generally explains the amplitude of the observed wave field even in the complicated ridge area.

2.1.4. Velocities. We compare velocities in our models to velocities derived for the onshore Franciscan, offshore Franciscan/San Simeon (paleoaccretionary complex assemblages of pre-Miocene age) and onshore Salinian (granitic batholith)

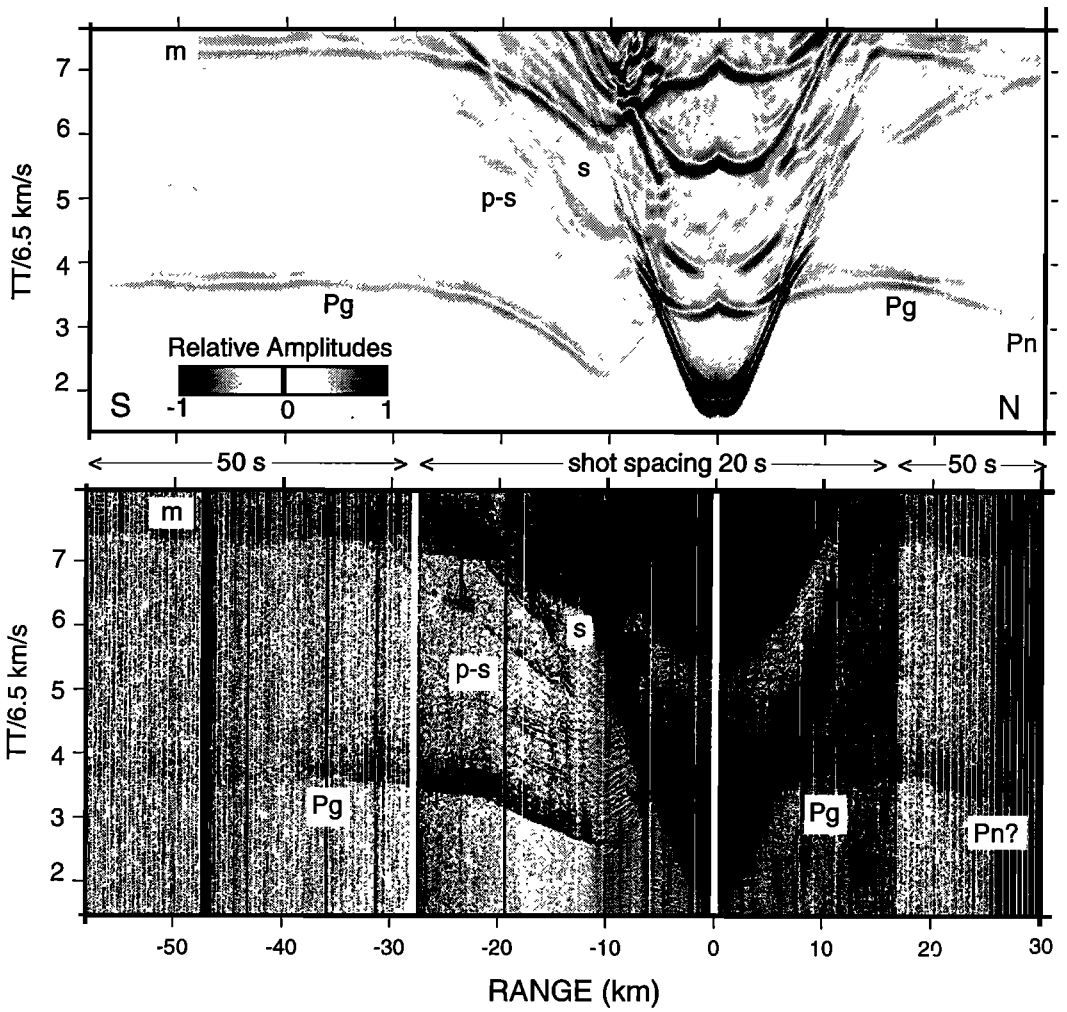

Figure 5. Amplitude plots of (top) synthetic and (bottom) observed record sections of OBH 17; m, multiple caused by reflection at the water surface directly above the instrument; S, shear wave through the ridge; p-s, P-to-S conversion at basement. For comparison see also the record section in Figure 2g.

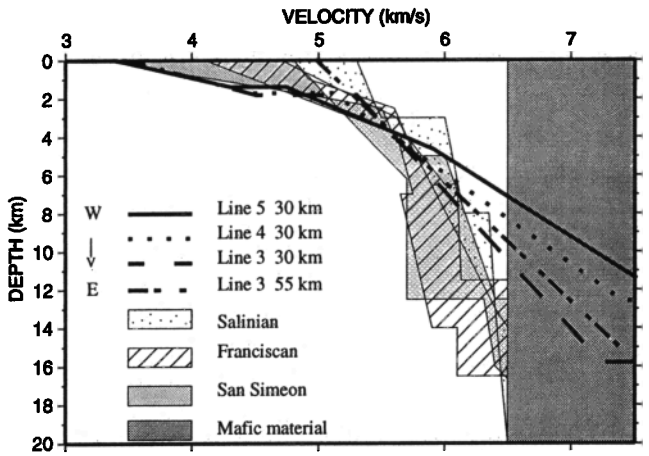

Figure 6. Velocity-depth profiles of lines 3S, 4, and 5 of the velocity models shown in Plate 1 (c)-(e). The resolution of our velocity models is best in the top 6 km and decreases with depth. The indicated regions (see legend) mark the range of velocities for Salinian terrane onshore [*Walter and Mooney*, 1982; *Howie et al.*, 1993], Franciscan terrane onshore [*Walter and Mooney*, 1982; *Howie et al.*, 1993; *Holbrook et al.*, 1996], and Patton/San Simeon terrane offshore [*Howie et al.*, 1993; *Holbrook et al.*, 1996]. All velocity profiles are normalized to the top of the basement as 0 km. Velocities between 6.5 to 7.5 kms^{-1} are too high for Salinian, Franciscan, or San Simeon/Patton terrane and represent mafic material or underlying oceanic crust.

terranes (Figure 6). Basement along lines 3S, 4, and 5 (south of the Mendocino transform fault) is likely composed of material similar to the Franciscan and San Simeon terranes. The velocity-depth profile for line 3S at km 30, representative of the western part of the Vizcaino block, has velocities in the upper crust typical of those for San Simeon/Patton terrane. In contrast, velocities at a given depth at km 55 are slightly higher and are consistent with Franciscan or Salinian terrane, which are typically 6-6.3 kms^{-1}. Velocities in the lower crust along line 3S, however, are too high to be accretionary complex material, and a tectonically or magmatically underplated mafic layer is likely. A reflection at 6-7 s twtt is apparent on a 1977 U.S. Geological Survey MCS reflection line located 10-20 km west of line 5 [*McCulloch*, 1987a; *Godfrey*, 1997]. Using our velocity-depth profile, this reflector coincides with the 6 kms^{-1} contour at about 9 km depth, supporting the interpretation of tectonically underplated oceanic crust.

2.2. Modeling the Gravity Data

We modeled free-air gravity anomalies recorded by the R/V *Ewing* along the MCS profiles and merged with the navigation at 1-min time intervals. The Eötvos correction was applied, and the 1980 theoretical gravity field was removed. Data correction procedures and instrumentation on the R/V *Ewing* are described by *Diebold* [1995]. Gravity data derived from satellite altimetry [*Sandwell and Smith*, 1997] supplement the ship-board measurements at the track ends. A 5-10 mGal shift of the global marine gravity data was necessary to overlap the data sets; this is within observed shifts between global marine gravity data and ship board measurements [*Sandwell and Smith*, 1997]. In addition to the free-air anomaly, we calculated a Bouguer anomaly by removing the effect of the topography and sediment layer by replacing them with material of average crustal density (2.75 gcm^{-3} in this study). The Bouguer anomaly reflects density variations beneath the sediment layer and can be compared to other gravity profiles with different topography and basin structure.

The main goals of the gravity modeling were to test and extend the velocity models, putting limits on the Moho where it is not imaged by the seismic data. We did not attempt to match the observed data exactly and focused on explaining long wavelength variations, which reflect density variations beneath the sediment layer. Starting gravity models incorporated bathymetry, changes in sediment thickness, and layer boundaries from the velocity model. The average velocity within layers of variable velocity was used to determine density. Velocity was converted to density using laboratory and field measurements summarized in Table 2. The crust was split into middle and lower crustal layers with densities of 2.75 gcm^{-3} and 2.9 gcm^{-3}. Lithospheric and asthenospheric densities were derived by adding density contrasts of 0.4 and 0.36 gcm^{-3} respectively to the density of the lower crust (Table 2). Two-dimensional gravity modeling and inversion to obtain the crust-mantle boundary was done with GM_SYS software (Northwest Geophysical Associates, Corvallis, Oregon), following the theory of *Talwani et al.* [1959]. RMS values for the models outlined in this study are summarized in Table 1.

2.2.1. Line 3S. We constrained the depth to the Moho at the northeastern end of line 3S to be 20 km based on a deep reflection observed on the MCS data at about 8 s twtt [*Henstock et al.*, 1996]. This event is nearly continuous on MCS line 3S from km 45-76 [*Henstock et al.*, 1996]. It is also seen on other profiles crossing the northeastern Vizcaino block [*Godfrey*, 1997; *Godfrey et al.*, this issue].

The Bouguer anomaly (Figure 7b) decreases by 150 mGal from west to east. This change is 3 times greater than the change in free-air gravity (50 mGal, Figure 7a). We interpret this signal to primarily reflect the change in Moho depth along the profile. Three different density models that all incorporate bathymetry and sediment thickness and which are compatible with the gravity data are shown in Figures 7c-7e. All 3 gravity models show (1) an east dipping, lower crustal layer between km 0 and 15 (dip <= 5°), (2) a transition zone between km 15 and 30 with a steeply dipping Moho (model I = 21°, model II = 30°, model III = 54°), (3) an abrupt lateral change in density at some depth in the crust or uppermost mantle between km 40 and 50. This density change is needed to account for a 20-mGal increase in the free-air gravity anomaly. Model I (Figure 7c) assumes a low-density body (2.55 gcm^{-3} versus 2.75 gcm^{-3}) at a shallow level

Table 2. Velocity-Density Conversion References

Material type	Density (gcm^{-3})	References
Sediment	2.0-2.3	*Nafe and Drake* [1957]
Franciscan	2.75	*Stewart and Peselnick* [1977]
Upper oceanic crust	2.75	*Christensen and Salisbury* [1975]
Lower oceanic crust	2.9	*Christensen and Mooney* [1995]
Upper mantle	3.3	based on 0.4 gcm^{-3} density contrast to lower crust [*Jachens and Griscom*, 1983]
Asthenosphere	3.26	based on -0.04 gcm^{-3} density contrast to upper mantle [*Jachens and Griscom*, 1983]

Densities were obtained by using the average velocities from the velocity models and converting to an average density using data from the appropriate reference.

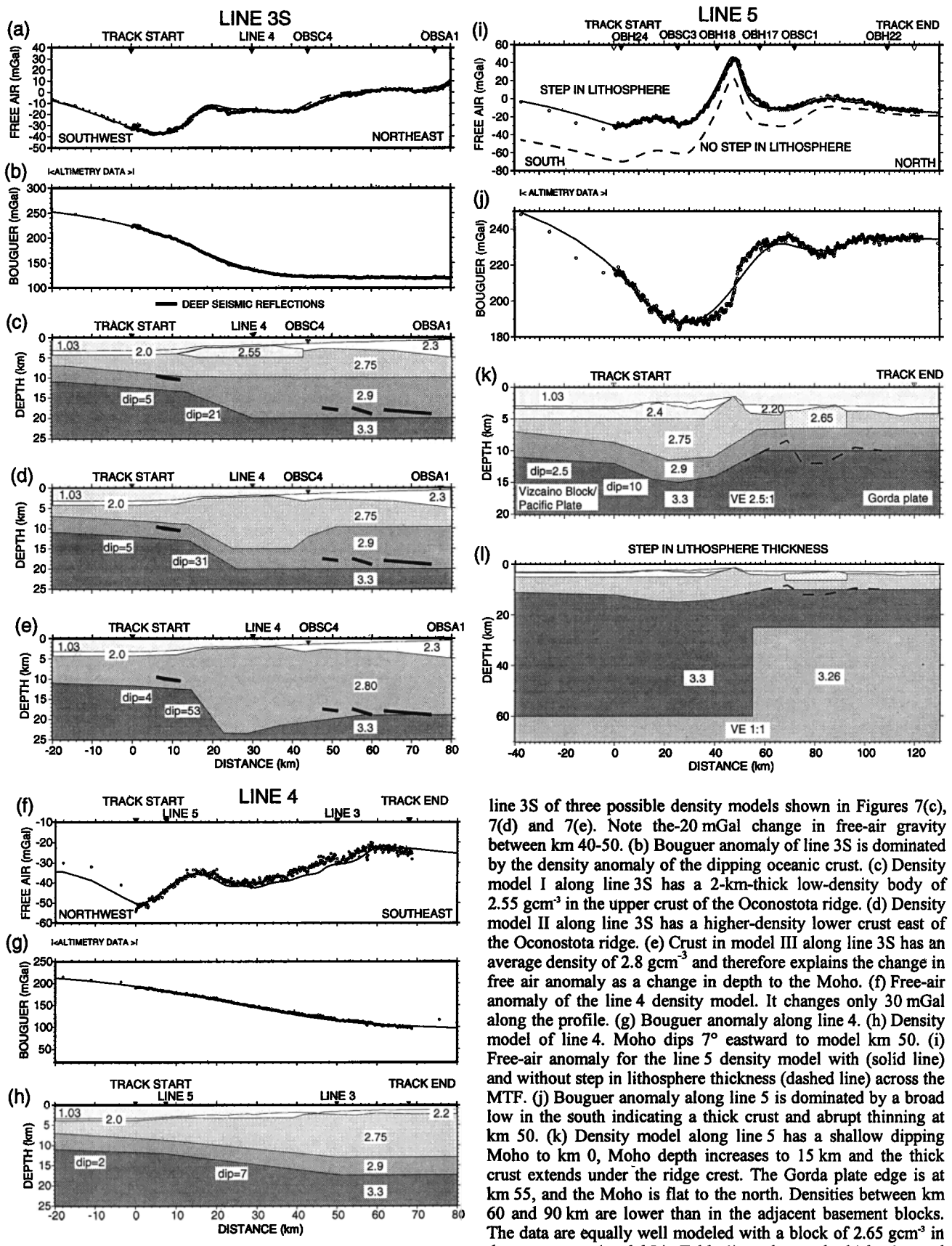

Figure 7. Observed (circles) and calculated (solid line) free air and Bouguer anomalies and density models for lines 3S, 4, and 5. Altimetry data extend the profiles at the track ends. Average block densities are given in gcm^{-3}. (a) Free-air anomaly along line 3S of three possible density models shown in Figures 7(c), 7(d) and 7(e). Note the-20 mGal change in free-air gravity between km 40-50. (b) Bouguer anomaly of line 3S is dominated by the density anomaly of the dipping oceanic crust. (c) Density model I along line 3S has a 2-km-thick low-density body of 2.55 gcm^{-3} in the upper crust of the Oconostota ridge. (d) Density model II along line 3S has a higher-density lower crust east of the Oconostota ridge. (e) Crust in model III along line 3S has an average density of 2.8 gcm^{-3} and therefore explains the change in free air anomaly as a change in depth to the Moho. (f) Free-air anomaly of the line 4 density model. It changes only 30 mGal along the profile. (g) Bouguer anomaly along line 4. (h) Density model of line 4. Moho dips 7° eastward to model km 50. (i) Free-air anomaly for the line 5 density model with (solid line) and without step in lithosphere thickness (dashed line) across the MTF. (j) Bouguer anomaly along line 5 is dominated by a broad low in the south indicating a thick crust and abrupt thinning at km 50. (k) Density model along line 5 has a shallow dipping Moho to km 0, Moho depth increases to 15 km and the thick crust extends under the ridge crest. The Gorda plate edge is at km 55, and the Moho is flat to the north. Densities between km 60 and 90 km are lower than in the adjacent basement blocks. The data are equally well modeled with a block of 2.65 gcm^{-3} in the upper crust (model I in Table 1) or alternately thickening and thinning lower crust (dashed line, model II in Table 1). (l) Same as density model in Figure (k), but incorporates a step in lithosphere according to the age contrast of Pacific and Gorda plates.

beneath the Oconostota ridge, as suggested by our velocity model. The observed Moho dip of 20° beneath the Oconostota ridge is a minimum value; a shallower dip would require unreasonable low-density values. Alternatively, the density contrast can be modeled by a relative density high in the lower crust east of model km 45 (model II, Figure 7d), which is compatible with the velocity model derived from the onshore-offshore seismic data [*Henstock et al.*, 1996]. Model III was determined from inversion of the gravity data for Moho position assuming no lateral density variations within the crust and illustrates the change in crustal thickness needed to fit this end-member case (Figure 7e). Since we do not expect a westward increase in crustal thickness and both models I and II are supported by seismic data, our preferred model is a combination of models I and II with relative weights presently poorly constrained.

2.2.2. Line 4. The free-air anomaly (Figure 7f) changes by only 40 mGal along the profile. The Bouguer anomaly decreases from west to east, reflecting the increase in Moho depth. Moho dip increases from 4° to 7° at km 8. Between km 8 and 50, Moho depth increases linearly from 12 to 17 km, and east of km 50, the Moho is flat. We did not force the models to agree at the intersections with lines 3S and 5, and therefore the mismatch between the models gives a qualitative measure of model uncertainty. A mismatch in Moho depth of about 3 km between the gravity models for lines 3S and 4 can be partly removed by introducing an additional low-density layer in the line 4 model upper crust, which supports the existence of an intermediate-velocity layer beneath the basement along line 4. We did not include this layer in our gravity model since it is only based on modeling the large-aperture data near OBH 24. The observed dip of 7° along the line 4 profile contrasts with the steep dip on line 3S in this region, suggesting that line 4 trends obliquely to the sharply dipping structure modeled on line 3S.

2.2.3. Line 5. The free-air gravity anomaly along line 5 is dominated by large anomalies over the Mendocino Ridge (50-70 mGals), over a bathymetric high on the Vizcaino block (10 mGal) and over a basement high on the Gorda plate (20 mGal) (Figure 7i). The Bouguer anomaly is dominated by the change in Moho depth south of the Gorda Escarpment, where a broad low of 50 mGal outlines the thick crust of the Vizcaino block (Figure 7j). In addition, the Bouguer gravity has a 10 mGal low between km 60 and 100.

The density model (Figures 7k and 7l) derived from the velocity model needed three changes to fit the data satisfactorily: (1) A northward dipping Moho (maximum dip 10°) beneath km 0 and 15, (2) on the Gorda plate, either a low-density block (Figure 7k) or, alternatively, thinning and thickening of the oceanic crust between km 70 and 100 (dashed line, Figure 7k), (3) a contrast in upper mantle densities corresponding to a lithosphere-asthenosphere boundary calculated from the age contrast [*Fowler*, 1990, p. 238] between the Gorda (5-6 Ma) and Pacific (27 Ma) plates.

3. Discussion

The density and velocity models along all three profiles indicate an abrupt increase in Moho dip at the western margin of the Oconostota ridge and a thickened upper crust within the Oconostota ridge. Along line 3S, the dip of the Moho changes abruptly from <5° at the western end of the profile to 20-30° (density models I and II, Figures 7c and 7d) over a distance of at most 16 km beneath the seaward boundary of the Vizcaino block and Oconostota ridge. Line 4 is entirely within the Vizcaino block in the region of the Oconostota ridge but trends obliquely to it. The part of line 5 that is south of the Mendocino transform fault also crosses the Oconostota ridge obliquely. The Moho kink modeled beneath the Oconostota ridge on lines 4 and 5 has true dips of 17° and 20°, respectively, when corrected for obliquity (Table 3). This is consistent with the minimum value of Moho dip modeled along line 3S (model I). If the Moho dip along Line 3S is in fact larger than 20°, it would imply an increase in Moho dip along strike, but this cannot be resolved with our data set. This Moho dip is much steeper than that observed beneath the accretionary complex anywhere in the active Cascadia subduction margin [*Tréhu et al.*, 1994, 1995; *Flueh et al.*, 1997; *Parsons et al.*, 1998], suggesting that the relict subduction boundary making up the western boundary of the Vizcaino block has been significantly deformed.

Northeast of the Moho kink on line 3S, the Moho flattens at a depth of about 20 km, and we observe a lateral density change within the crust 10-15 km east of the Oconostota ridge. This density change can be modeled either as a change in crustal material, as thinning of the upper crust, or as thickening of the lower crust (or some combination thereof) and coincides with an apparent change in crustal reflectivity and the appearance of a deep reflector to the northeast [*Henstock et al.*, 1996; *Godfrey*, 1997; *Godfrey et al.*, this issue]. In contrast, no regionally coherent deep reflections are observed on any of the profiles crossing the northwestern region of the Vizcaino block.

Beneath the Gorda Escarpment, the density model of line 5 (Figure 7l) indicates abrupt crustal thinning to the north. Matching the long-wavelength data requires that the Mendocino transform fault continues vertically through the plate lithospheres, similar to *Wilson's* [1989] gravity models across the Mendocino Ridge west of 126°. The high velocities and lack of a crustal root beneath the Mendocino Ridge suggest that it was formed by uplift and tilting of the Vizcaino block in response to Pacific-Gorda compressive forces.

The low-density block and/or Moho variation beneath the basement high on the Gorda plate modeled on line 5 (Figure 7k) are not imaged in the large-aperture seismic data. Neither of our density models are compatible with the high being a flexural bulge, as this would result in a relative density high. The basement high may have formed either through thrusting and thickening of the Gorda crust in response to north-south compression, similar to the crustal thickening beneath the

Table 3. Geometry of Lines and Apparent and True Dips of Moho Kink

Line	Apparent Moho Dip Along Trend of Line, deg	Angle of Line to N45°E, deg	True Dip of Moho Kink , deg
3	20-30 (Figures 7c and 7d)	0	20-30
4	7 (Figure 7f)	58	17
5	10 (Figure 7k)	45	20

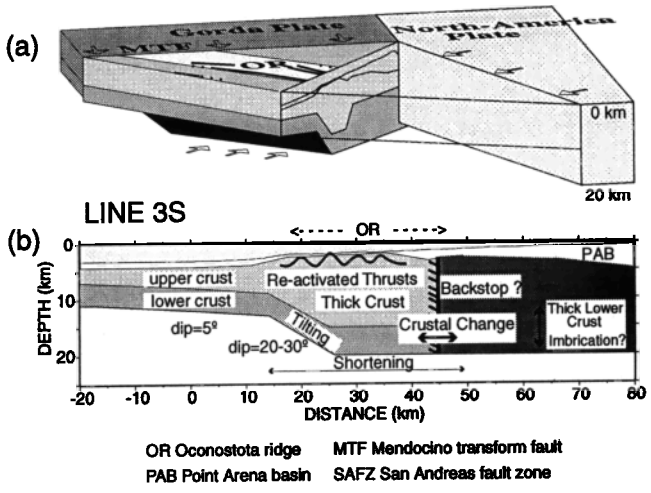

Figure 8. (a) Three-dimensional cartoon of the crustal structure in the northwestern part of the Vizcaino block. The Moho dip abruptly increases to about 20° in the north and 20-30° to the south. The section ends at the southwest-northeast trending line 3S, where our data set ends. The lower crust is shown in dark gray and anything above in lighter gray. The approximate region of the Oconostota ridge is marked in light gray. Mapped basement ridges after *Godfrey* [1997] are solid lines, dotted where uncertain. Arrows show direction of compression. (b) Sketch of line 3S, which is a cross section of the Vizcaino block. We suggests that compression shortened the lower crust, kinked it, and thickened the upper crust along preexisting thrust faults; faulting and folding the upper crust and sediments. At model km 45, we see a crustal change and possibly thickening of the oceanic crust or mafic layer.

Oconostota ridge, or it may be a relict structure created by an excess of magmatism at the spreading center. We prefer the first explanation because the basement high corresponds to a southwest-northeast trending seafloor ridge visible in Gloria sidescan data [*EEZ-SCAN84 Scientific Staff*, 1986], which is approximately coincident with a persistant lineation in the pattern of Gorda plate seismicity and with the aftershock zone of a magnitude 7 intraplate event that occurred in November 1980 [*Smith et al.*, 1993].

4. Tectonic Implications

Our primary result is that the paleosubduction zone preserved along the seaward edge of the Vizcaino block has been significantly deformed. This is suggested by the increase in Moho dip from about 5° west of the Oconostota ridge to 20-30° beneath the western margin of the Vizcaino block and the Oconostota ridge. This dip is consistent on all three profiles when the apparent dip is corrected for the obliquity of the profiles relative to the northwest trend of the structure indicated by global marine gravity (Plate 1b and Table 3) and multichannel seismic data [*McCulloch*, 1987a; *Godfrey*, 1997]. Crustal thickness farther east is approximately constant, resulting in a kink in the Moho that strikes about N45°W and underlies the western margin of the Vizcaino block (Figure 8a). This type of structure is not observed farther north in Cascadia but is observed on many crossings farther south on the California continental margin [e.g. *Trèhu*, 1991; *Meltzer and Levander*, 1991; *Howie et al.*, 1993; *Holbrook et al.*, 1996; *Miller et al.*, 1992, 1996]. It is not observed, however, across the southwestern boundary of the Vizcaino block [*Henstock et al.*, 1997]. Offshore central California, the Moho kink has been attributed to crustal imbrication on thrust faults and/or deformation along buried transform faults.

In order to reconstruct the tectonic processes that lead to the Moho kink and thickened crust, we look at several reflection profiles crossing the Oconostota ridge (red and gray lines, Plate 1a). These profiles show a series of basement ridges overlain by folded sediments (Figures 3b, 4, and 9). Because of their similarity to ridges seen in the active accretionary prism of the Cascadia subduction zone [*Goldfinger et al.*, 1992; *Pratson and Haxby*, 1996], *Godfrey* [1997] suggested that these ridges formed in an accretionary complex during the subduction regime and were later reactivated. This outer zone of the accretionary wedge was relatively young, thin, weakened by preexisting faults and thermally weakened by the subducted Farallon ridge beneath it (Plate 1b). It is therefore not surprising that deformation was focused in this region. Reactivation of these thrust folds clearly continued until relatively recently (Figures 4 and 9), but the absence of seismicity or of northwest trending ridges on the seafloor suggests that they are not active today. We speculate that the Moho kink represents shortening of the lower crust in response to the same compression that reactivated the thrust faults and thickened the overlying accretionary complex material (Figure 8b). Placing constraints on the time of initiation and cessation of reactivation, however, is difficult because of the small number of drill holes in the region, the discontinuous nature of the seismic reflections, the presence of intervening basement ridges, and active seafloor erosion (Figures 4 and 9). High resolution seismic data near the ODP Site 1022 (yellow circle, Plate 1a) suggest that deformation ceased at about 3.4 Ma (Lyle et al., 1997).

Another significant result of our modeling is the apparent thinning of the upper crust and/or thickening of the lower-crust northeast of km 45 on line 3S (Figure 8b). The trend of this change in distribution of upper and lower-crustal material is presently poorly constrained because of sparse seismic data and because the wavelength of the gravity anomaly on which this feature is based on is too short to be resolved in global marine gravity data. Based on a general northwest-trending pattern in Neogene structures and gravity data (Plate 1a and 1b), we assume a northwest trend. Possible explanations for the change in crustal structure include (1) the same compressive event that resulted in the Moho kink, which might have imbricated and thickened the lower crust, (2) extension and magmatic underplating in response to subduction of the Pacific-Farallon ridge, and (3) lateral variations in crustal structure within the forearc formed during Farallon-North America plate subduction. We speculate that higher-velocity and density material 10-15 km east of the Oconostota ridge may represent a mechanical backstop that contributed to localizing deformation beneath the Oconostota ridge (Figure 8b).

A third result of our modeling is a new constraint on the composition of material forming the Mendocino Ridge and the geometry of changes in crustal thickness associated with the Gorda Escarpment. The model for line 5 shows that the velocity and density within the Mendocino Ridge are not resolvable different from that within the basement of the adjacent Vizcaino block. Combined with stratigraphic evidence for uplift and tilting of the Mendocino Ridge [*Silver*, 1971; *Godfrey et al.*, this issue], this suggests that the Mendocino Ridge east of 126° is

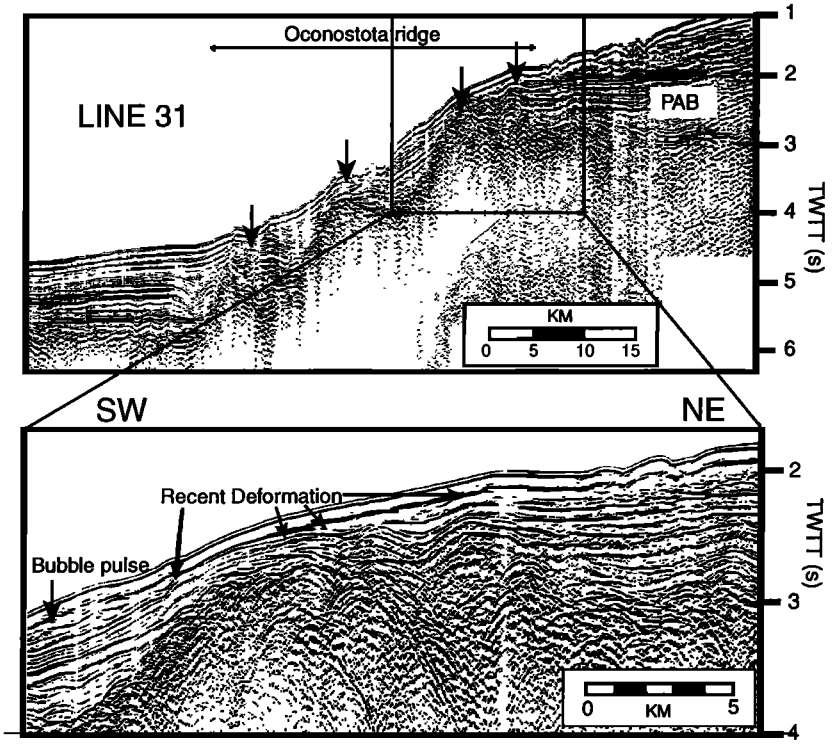

Figure 9. Migrated seismic reflection profile collected by the USGS in 1977 [*McCulloch*, 1987a; *Godfrey*, 1997, *Godfrey et al.*, this issue]. Arrows mark the location of the cross cutting basement ridges seen throughout the northwestern Vizcaino block (Plate 1a). Bottom figure shows recent sediment deformation above one of the N45°W trending thrust faults.

constructed from tectonically uplifted accretionary complex material. We cannot, however, rule out tectonic mixing of accretionary complex rocks and uplifted oceanic crust. The configuration of the Moho beneath the Gorda Escarpment indicates that the Mendocino Ridge is not underlain by a crustal root and has therefore been formed and maintained dynamically by compressive forces across the Pacific-Gorda plate boundary. Reported subsidence of the Mendocino Ridge since 5 Ma [*Fisk et al.*, 1993] does not contradict our observations but indicates that compression is decreasing over time. Timing of the uplift and subsequent partial subsidence of the Mendocino Ridge in this region is likely related to changes in the amount of compression across the Mendocino transform fault and to the degree to which compression is accommodated by intraplate deformation.

The formation of the Oconostota ridge and underlying Moho kink and the formation of the Gorda Escarpment and adjacent basement ridge both suggest compressive stress in the Vizcaino block during and/or after its accretion to the Pacific plate, but stratigraphic constraints on the timing of compression are poor. Because these features likely occurred along preexisting faults, the direction of the maximum compressive stress is also poorly constrained.

In order to obtain additional insights into when the deformation or uplift may have occurred, we return to the plate tectonic history summarized in Figure 1. In Figure 10, we show the lithospheric age contrast across the Pacific-Juan de Fuca/Gorda plate boundary and the component of normal stress across the Mendocino transform and San Andreas fault zones and relate these parameters to the tectonic history of the Vizcaino block as inferred from our crustal models. Figure 10 shows that compression across the Mendocino transform was small during a relative stable phase of Pacific plate motion from about 19 to 10 Ma, increased slightly in the period between 10 and 6 Ma, and has been relatively strong since then. It also shows that the lithospheric age contrast across the Mendocino transform near its intersection with the Oconostota ridge flipped 12.5 to 10 Ma and that Pacific-North America relative plate motion was transtensional prior to ~3.5 Ma. In spite of strong normal forces across both plate boundaries at the present time, the lack of seismicity (Plate 1a) and sediment deformation since about 3.4 Ma [*Lyle et al.*, 1997] indicates that the Vizcaino block is not deforming internally under the current stress regime. Since at least 3 Ma, north-south compression has been absorbed internally by the Gorda plate [*Wilson*, 1989] and east-west compression has been accommodated farther east, within the Point Arena basin [*Ondrus*, 1997].

We suggest that most of the internal deformation of the Vizcaino block resulted from transpression in response to Pacific-Juan de Fuca/Gorda plate compression (dark gray shaded regions, Figure 10) when the normal stresses across the bounding transforms were relatively large (about 6-3 Ma) and/or when the Vizcaino block lower crust was very young, weak, and juxtaposed against the older Juan de Fuca plate to the north (18-12.5 Ma). Internal deformation is less likely in the late Miocene (6-12 Ma), when both north-south compression and the lithospheric age contrast were relatively small (light gray shaded region, Figure 10). The observation that internal deformation of the Vizcaino block seems to have stopped and been transferred to the Gorda plate, even though the compressive stress within the

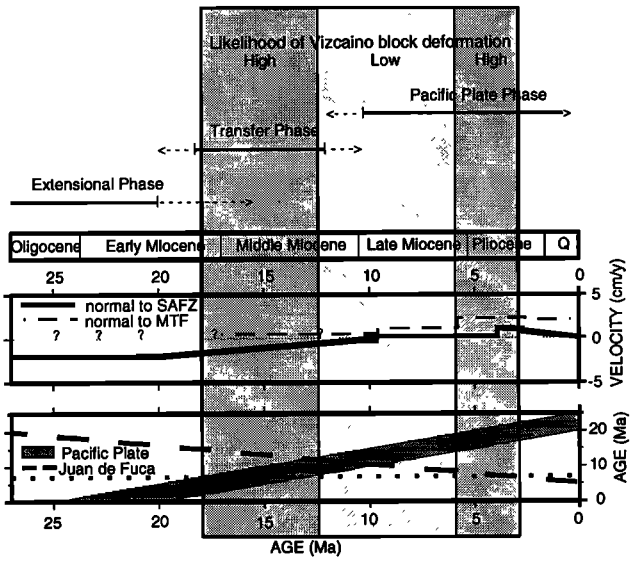

Figure 10. Factors influencing the likelihood of compressional deformation in the Vizcaino block. At the top, solid lines mark lower age and dashed lines mark the upper age limit of the Vizcaino block phases sketched in Figure 1. Normal forces across the transforms are calculated from stage poles near the Oconostota ridge-MTF intersection [*Wilson*, 1993] and just south of the Mendocino triple junction region [*Harbert and Cox*, 1989] and are projected to a fault at 90° (MTF) and 319.5° (SAFZ). The strike of the San Andreas fault north of Point Arena (since 3.5 Ma) is about 330°, and therefore the present plate motion normal to the San Andreas fault is negligible. Velocity normal to the MTF of the Pacific-Farallon plates between 19 and 10 Ma was relatively small and uncertain. Age of the Farallon and later Juan de Fuca plate [*Engebretson et al.*, 1985] are estimates assuming a constant spreading rate. Pacific plate age is indicated by the dark gray region which marks the possible time span of ridge cessation at about 25 to 20 Ma. The horizontal dotted line marks the onset of Gorda plate deformation (minimum age). When considering the possible Vizcaino block deformation in the early Miocene, we assume that the then young Pacific plate deformed at about the same age. Light gray area indicates small likelihood for Vizcaino block deformation; dark gray areas indicate times of likely deformation.

Pacific plate should be larger now than at any time in the past history of triple junction interaction, suggests that lithospheric age has a major effect on intraplate deformation.

5. Conclusions

Our data show evidence for significant deformation of the crust in the northwestern part of the Vizcaino block. The internal deformation resulted primarily from transpression in response to Pacific-Juan de Fuca plate compression when normal stresses across the bounding transforms were relatively large (6-3.4 Ma) and/or when the Vizcaino block was considerably younger and weaker than the adjoining Juan de Fuca plate (18-12.5 Ma). This compression appears to have reactivated preexisting crustal faults, thickened the crust of the Oconostota ridge, and formed a kink in the Moho beneath the northwestern margin of the Vizcaino block. It also tilted and uplifted the Vizcaino block at its northern margin, forming the Gorda Escarpment and adjacent basement ridge. A lateral change in structure is observed to the northeast of the Oconostota ridge, but it is unclear if this is a product of the same deformation or was a preexisting feature and therefore acted as a backstop during the deformation. Deformation within the Vizcaino block appears to have ceased and shifted to the Gorda plate sometime prior to 3 Ma. We suggest that the spatial and temporal shifts of the primary locus of deformation resulted from changes in relative motions across the Pacific, Juan de Fuca/Gorda and North America plate boundaries combined with changes in lithospheric age and age contrast across these boundaries.

Acknowledgments. We thank the participants of the Mendocino Triple Junction Seismic Experiment: Special thanks go to the crews of the R/V *Ewing* and R/V *Wecoma* and to Ken Peals, Beecher Wooding and Greg Miller for running the OBS/OBHs. Thanks to T. Henstock, who provided the depth-migrated MCS profile for line 3S, and to A. S. Meltzer, who provided the time-migrated profile for line 5. Reviews by T. Brocher, R. Keller, and K. Miller greatly improved this manuscript. B. Leitner gratefully acknowledges the support of J. L. Nábelek and D. Eberhart Phillips. Gerald Connard at Northwest Geophysical Associates (Corvallis, Oregon) provided a test copy of GM_SYS for Unix. Plots were created using GMT [*Wessel and Smith*, 1995]. This research was supported by NSF grants 9219870-EAR and 9527011-EAR to Oregon State University and EAR-9218209 to Stanford University.

References

Atwater, T., Implications of plate tectonics for the Cenozoic tectonic evolution of western North America, *Geol. Soc. Am. Bull.*, *81*, 3513-3536, 1970.

Atwater, T., Plate tectonic history of the northeast Pacific and western North America, in *The Geology of North America*, vol. N, *The Eastern Pacific Ocean and Hawaii*, edited by E. L. Winterer, D. M. Hussong, and R. W. Decker, pp. 21-72, Geol. Soc. of Am., Boulder, Colo., 1989.

Atwater, T., and J. Severinghaus, Tectonic maps of the northeast Pacific, in *The Geology of North America*, vol. N, *The Eastern Pacific Ocean and Hawaii*, edited by E. L. Winterer, D. M. Hussong, and R. W. Decker, pp. 15-20, Geol. Soc. of Am., Boulder, Colo., 1989.

Blake, M. C., Jr., and D. L. Jones, The Franciscan assemblage and related rocks in northern California: A reinterpretation, *The Geotectonic Development of California*, edited by W. G. Ernst, pp. 307-328, Prentice-Hall, Englewood Cliffs, N.J., 1981.

Bohannon, R. G., and T. Parsons, Tectonic implications of post-30 Ma Pacific and North American relative plate motions, *Geol. Soc. Am. Bull.*, *107*, 937-959, 1995.

Bonatti, E., Vertical tectonism in oceanic fracture zones, *Earth Planet. Sci. Lett.*, *37*, 369-379, 1978.

Braunmiller, J., B. Leitner, J. Nábelek, and A. M. Tréhu, Location and source parameters of the 19 June 1994 (M_w=5.0) offshore Petrolia, California, earthquake, *Bull. Seismol. Soc. Am.*, *87*, 272-276, 1997.

Castillo, D. A., and W. L. Ellsworth, Seismotectonics of the San Andreas fault system between Point Arena and Cape Mendocino in northern California: Implications for the development and evolution of a young transform, *J. Geophys. Res.*, *98*, 6543-6560, 1993.

Christensen, N. I., and W. D. Mooney, Seismic velocity structure and composition of the continental crust: A global view, *J. Geophys. Res.*, *100*, 9761-9788, 1995.

Christensen, N. I., and M. H. Salisbury, Structure and constitution of the lower oceanic crust, *Rev. Geophys.*, *13*, 57-86, 1975.

Christeson, G. L., Y. Nakamura, K. D. McIntosh, and P. Stoffa, Effect of shot interval on ocean bottom seismograph and hydrophone data, *Geophys. Res. Lett.*, *23*, 3783-3786, 1996.

Cox, A., and D. Engebretson, Change in motion of Pacific plate at 5 Myr BP, *Nature*, *313*, 472-474, 1985.

Denlinger, R. P., A model for large-scale plastic yield of the Gorda deformation zone, *J. Geophys. Res.*, *97*, 15415-15423, 1992.

Dickinson, W. R., and W. S. Snyder, Geometry of triple junctions related to San Andreas transform, *J. Geophys. Res.*, *84*, 561-572, 1979.

Diebold, J., *R/V Ewing leg EW9412*, Lamont-Doherty Earth Obs., Columbia Univ., Palisades, N.Y., 1995.

Drake, D. E., D. A. Cacchione, J. V. Gardner, D. S. McCulloch and D.

Masson, Morphology and growth history of Delgada fan: Implications for the Neogene evolution of Point Arena basin and the Mendocino triple junction, *J. Geophys. Res., 94,* 3139-3158, 1989.

Duncan, R. A., and D. A, Clague, Pacific plate motion recorded by linear volcanic chains, in *The Ocean Basins and Margins*, vol. 7A, edited by A. E. M. Nairn, F. G. Stehli, and S. Uyeda, pp. 89-121, New York, Plenum, 1985.

Duncan, R. A., M. R. Fisk, A. G. Carey Jr., D. Lund, L. Douglas, D. S. Wilson, D. Krause, R. Stewart, and C. G. Fox, Origin and emergence of Mendocino Ridge (abstract), *Eos Trans. AGU, 75 (44),* Fall Meet. Suppl., 475, 1994.

EEZ-SCAN 84 Scientific Staff, Atlas of the exclusive economic zone, western conterminous United States, *U.S. Geol. Surv. Misc. Invest., I-1792*, 152 pp., 1986.

Engebretson, D. C., Cox, and R. G. Gordon, Relative motions between oceanic and continental plates in the Pacific Basin, *Geol. Soc. Am. Spec. Pap., 206,* 59 pp., 1985.

Fernandez, L. S., and R. N. Hey, Late Tertiary tectonic evolution of the seafloor spreading system off the coast of California between the Mendocino and Murray fracture zones, *J. Geophys. Res., 96,* 17955-17979, 1991.

Fisk, M. R., R. A. Duncan, C. G. Fox, and J. B. Witter, Emergence and petrology of the Mendocino Ridge, *Mar. Geophys. Res.,15*, 283-296, 1993.

Flueh, E., M. Fisher, D. Scholl, T. Parsons, U. ten Brink, D. Klaeschen, N. Kukowski, A. Tréhu, J. Childs, J. Bialas, and N. Vidal, Scientific teams analyze earthquake hazards of the Cascadia subduction zone, *Eos Trans. AGU, 78,* 153-157, 1997.

Fowler, C. M. R., *The solid earth*, An introduction to global geophysics, 472 pp., Cambridge University Press, 1990.

Godfrey, N. J., Crustal structure of northern California, Ph.D. thesis, Stanford University press, Stanford, 177 pp., 1997.

Godfrey, N. J., A. S. Meltzer, S. L. Klemperer, A. M. Tréhu, B. Leitner, S. H. Clarke Jr. and A. Ondrus, Evolution of the Gorda Escarpment, San Andreas fault, and Mendocino triple junction from multichannel seismic data collected across the northern Vizcaino block, offshore northern California, *J. Geophys. Res.*, this issue.

Goldfinger, C., L. D. Kulm, R. S. Yeats, B. Appelgate, M. E. MacKay, and G. F. Moore, Transverse structural trends along the Oregon convergent margin; Implications for Cascadia earthquake potential and crustal rotations, *Geology, 10*, 141-144, 1992.

Graham, S. A., and W. Dickinson, Evidence for 115 kilometers of right slip on the San Gregori-Hosgri fault trend, *Science, 199,* 179-181, 1978.

Griscom, A., and R. C. Jachens, Tectonic history of the north portion of the San Andreas fault system, California, inferred from gravity and magnetic anomalies, *J. Geophys. Res., 94,* 3089-3099, 1989.

Harbert, W., and A. Cox, Late Neogene motion of the Pacific plate, *J. Geophys. Res., 94*, 3052-3064, 1989.

Henstock, T. J., A. Levander, and the Mendocino Working Group, Images of the Mendocino and San Andreas transforms in the Mendocino triple junction region: Continous seismic profiling across the continental margin (abstract), *Eos Trans. AGU*, 77 (46), Fall Meet. Suppl., F741, 1996.

Henstock, T. J., A. Levander, and J. A. Hole, Deformation in the lower crust of the San Andreas fault system in northern California, *Science, 278*, 650-653, 1997.

Holbrook, W. S., T. M. Brocher, U. S. ten Brink, and J. A. Hole, Crustal structure of a transform plate boundary: San Francisco Bay and the central California continental margin, *J. Geophys. Res., 101,* 22311-22334, 1996.

Hoskins, E. G., and J. R. Griffiths, Hydrocarbon potential of northern and central California offshore, *Future Petroleum Provinces of the United States, Marine Geology and Potential, edited by I. H. Cram, AAPG Mem., 15*, 212-228, 1971.

Howie J. M., K. C. Miller, and W. U. Savage, Integrated crustal structure across the south central California margin: Santa Lucia escarpment to the San Andreas fault, *J. Geophys. Res., 98*, 8173-8196, 1993.

Jachens, R. C., and A. Griscom, Geometry of the Gorda plate beneath northern California, *J. Geophys. Res., 88,* 9375-9392, 1983.

Krause, D. C., H. W. Menard, and S. M. Smith, Topography and lithology of the Mendocino Ridge, *J. Mar. Res., 22,* 236-249, 1964.

Kulm, L. V. D., R. von Huene, J. R. Duncan, J. C. J. Ingle, S. A. Kling, L. F. Musich, D. J. W. Piper, R. M. Pratt, H. Scrader, O. E. Weser, and S. W. J. Wise, Site 173, *Initial Rep. Deep Sea Drill. Proj., 18,* 31-62, 1973.

Lendl, C., Finite difference wavefield modeling of large-aperture data from the 1993 Mendocino Triple Junction Seismic Experiment, master thesis, 163 pp., Oreg. State Univ., Corvallis, 163, 1996.

Lendl, C., A. M Tréhu, J. A. Goff, A. R. Levander, and B. C. Beaudoin. Synthetic seismograms through synthetic Franciscan: Insights into factors affecting large-aperture seismic data. *Geophys. Res. Lett., 24,* 3317-3320, 1997.

Lonsdale, P., Structural patterns of the Pacific floor offshore of Peninsular California, in *Gulf and Penisular Pprovinces of the Californias,* edited by P. Dauphin, J. Ness and B. Simoneit, *AAPG Mem., 47*, 87-125, 1991.

Lyle, M., I. Koizumi, C. Richter, and the Shipboard Scientific Party, *Proceedings of the Ocean Drilling Program: Initial Reports, V. 167,* Ocean Drill. Program, College Station, Tex., 1997.

Mattinson, J. M., Age, origin, and thermal histories of some plutonic rocks from the Salinian block of California, *Contrib. Mineral. Petrol., 67,* 233-245, 1978.

McCrory, P. A., D.S. Wilson, J.C. Ingle Jr., and R.G. Stanley, Neogene geohistory analysis of Santa Maria Basin, California, and its relationship to transfer of central California to the Pacific plate, *U.S. Geol. Surv. Bull., J,* 1-38, 1995.

McCulloch, D. S., The Vizcaino block south of the Mendocino triple junction, northern California, *Tectonics, Sedimentation and Evolution of the Eel River and Associated Basins of northern California, Proceedings of a Symposium*, edited by H. Schymiczek and R. Suchland, pp. 129-137, San Joaquin Geol. Soc. Misc. Publ., Bakersfield, Cal., 1987a.

McCulloch, D. S., Regional geology and hydrocarbon potential of offshore central California, in *Geology and Resource Potential of theContinental Margin of Western North America and Adjacent Ocean Basin s- Beaufort Sea to Baja California, Earth Sci. Ser.,* vol. 6, edited by D. W. Scholl, A. Grantz and J. G. Vedder, pp. 353-401, Circum-Pac. Counc. for Energy and Miner. Resour., Houston, Tex., 1987b.

McCulloch, D. S., Evolution of the offshore central California margin, in *The Geology of North America,* vol. N, *The Eastern Pacific Ocean and Hawaii,* edited by E. L. Winterer, D. M. Hussong, and R. W. Decker, pp. 439-470, Geol. Soc. of .Am., Boulder, Colo., 1989.

McLaughlin R. J., S. A. Kling, R. Z. Poore, K. McDougall, and E. C. Beutner, Post-middle Miocene accretion of Franciscan rocks, northwestern California, *Geol. Soc. Am. Bull., 93*, 595-605, 1982.

McLaughlin, R. J., W.V. Sliter, N. O. Frederiksen, W. P. Harbert, and D. S. McCulloch, Plate motions recorded in Tectonostratigraphic terranes of the Franciscan complex and evolution of the Mendocino triple junction, northwestern California, *U.S. Geol. Surv. Bull., 1997,* 60 pp., 1994.

McLaughlin, R. J., W.V. Sliter, D.H. Sorg, P.C. Russell, and A.M. Sarna-Wojcicki, Large-scale right-slip displacement on the East San Francisco Bay region faults system, California: Implications for location of late Miocene to Pliocene Pacific plate boundary, *Tectonics, 15*, 1-18, 1996.

Meltzer, A.S., and A. R. Levander, Deep crustal reflection profiling offshore southern central California margin, *J .Geophys. Res., 96,* 6475-6491, 1991.

Miller, K.C., J. M. Howie, and S. D. Ruppert, Shortening within underplated oceanic crust beneath the central California margin, *J. Geophys. Res., 97*, 19961-19980, 1992.

Miller, K. C., M. Dober, F. Hua, and R. G. Bohannon, Crustal gravity models along seismic reflection profiles, California Continental Borderland (abstract), *Eos Trans. AGU, 77 (46),* Fall Meet. Suppl., F737, 1996.

Nafe, J. E., and C. L. Drake, Variation with depth in shallow and deep marine sediments of porosity, density and the velocities of compressional and shear waves, *Geophysics, 22*, 523-552, 1957.

Nicholson, C., C. Sorlien, T. Atwater, J. Crowell, and B. Luyendyk, Microplate capture, rotation of the western Transverse Ranges, and initiation of the San Andreas transform as a low-angle fault system, *Geology, 22,* 491-495, 1994.

Ondrus, A., Deformation of the Point Arena basin and the location of the San Andreas Fault Zone, offshore northern California, M.S. thesis, 46 pp., Lehigh Univ., Bethlehem, Pa., 1997.

Parsons, T., A. M. Tréhu, J. H. Luetgert, F. Kilbride, K. Miller, R. E. Wells, M. A. Fisher, N. I. Christensen, U. S. ten Brink, E. Flueh, and W. D. Mooney, A new view into the Cascadia subduction zone and volcanic arc: Implications for earthquake hazards along the Washington margin, *Geology, 26,* 199-292, 1998.

Pratson, L. F., and W. F. Haxby, What is the slope of the U. S. continental slope?, *Geology, 24,* 3-6, 1996.

Riddihough, R. P., Gorda plate motions from magnetic anomaly analysis, *Earth Planet. Sci. Lett., 51,* 163-170, 1980.

Riddihough, R. P., Recent movements of the Juan de Fuca plate system, *J. Geophys. Res., 89,* 6980-6994, 1984.

Rodrigues, D. and P. Mora, Analysis of a finite difference solution to the three-dimensional elastic wave equation, paper presented at 67nd. Annual International Meeting, Soc. for Explor. Geophys, 1992.

Sandwell, D. T., and W. H. F. Smith, Marine gravity anomaly from Geosat and ERS 1 satellite altimetry, *J. Geophys. Res., 102,* 10039-10054, 1997.

Sedlock, R. L., and D. H. Hamilton, Late Cenozoic tectonic evolution of southwestern California, *J. Geophys. Res., 96,* 2325-2351, 1991.

Severinghaus, J., and T. Atwater, Cenozoic geometry and thermal state of the subducting slabs beneath western North America, in B. P. Wernicke, *Basin and Range Extensional Tectonics Near the Latitude of Las Vegas, Nevada, edited by Geol. Soc. of Am. Mem., 176,* 1-22, 1990.

Silver, E. A., Tectonics of the Mendocino triple junction, *Geol. Soc. Am. Bull., 82,* 2965-2978, 1971.

Smith, S. W., J. S. Knapp, and R. C. McPherson, Seismicity of the Gorda plate, structure of the continental margin, and an eastward jump of the Mendocino triple junction, *J. Geophys. Res., 98* , 8153-8171, 1993.

Stewart, R., and L. Peselnick, Compressional velocities in dry Franciscan rocks to 8 kbar and 300°C, *J. Geophys. Res., 83,* 2027-2039, 1977.

Stoddard, P. R., A kinematic model for the evolution of the Gorda plate, *J. Geophys. Res., 92* , 11524-11532, 1987.

Talwani, M., J. L. Worzel, and M. Landisman, Rapid gravity computations for two-dimensional bodies with application to the Mendocino submarine fracture zone, *J. Geophys. Res., 64,* 49-59, 1959.

Tréhu, A. M., Tracing the subducted oceanic crust beneath the central California continental margin: Results from ocean bottom seismometers deployed during the 1986 Pacific Gas and Electric EDGE Experiment, *J. Geophys. Res., 96* , 6493-6506, 1991.

Tréhu, A. M., I., Asudeh, T. M. Brocher, J. H. Luetgert, W. D. Mooney, and J. L. Nábelek, Crustal architecture of the Cascadia forearc, *Science, 266,* 237-242, 1994.

Tréhu, A. M., and the Mendocino Working Group, Pulling the rug out from under California: Seismic images of the Mendocino triple junction region, *Eos Trans. AGU, 76,* 369, 380-381, 1995.

Walter, A. W., and W. D. Mooney, Crustal structure of the Diablo and Gabilan Ranges, central California: A reinterpretation of existing data, *Bull. Seismol. Soc. Am., 72,* 1567-1590, 1982.

Wessel, P., and W. H. F. Smith, New version of the generic mapping tools released, *Eos Trans. AGU, 76,* 329, 1995.

Wilson, D. S., A kinematic model for the Gorda deformation zone as a diffuse southern boundary of the Juan de Fuca plate, *J. Geophys. Res., 91,* 10259-10269, 1986.

Wilson, D. S., Tectonic history of the Juan de Fuca ridge over the last 40 million years, *J. Geophys. Res., 93,* 11863-11876, 1988.

Wilson, D. S., Deformation of the so-called Gorda plate, *J. Geophys. Res., 94,* 3065-3075, 1989.

Wilson, D. S., Confidence intervals for motion and deformation of the Juan de Fuca plate, *J. Geophys. Res., 98,* 16053-16071, 1993.

Wilson, D. S., R. N. Hey, and C. Nishimura, Propagation as a mechanism of orientation of the Juan de Fuca Ridge, *J. Geophys. Res., 89,* 9215-9225, 1984.

Zelt, C. A., and R. B. Smith, Seismic traveltime inversion for 2-D crustal velocity structure, *Geophys. J. Int., 108,* 16-34, 1992.

Nicola J. Godfrey, Department of Earth Sciences, University of Southern California, Los Angeles, Ca 90089.

Beate Leitner, Institute of Geological and Nuclear Sciences, Dunedin Research Center, Private Bag 1930, Dunedin, New Zealand.

Anne M. Tréhu, College of Oceanic and Atmospheric Sciences, Oregon State University, Corvallis, OR, 97331. (email: nicola@usc.edu; beate@eos.otago.ac.nz ; trehu@oce.orst.edu)

(Received November 5, 1997; revised May 1, 1998;
accepted June 9, 1998.)